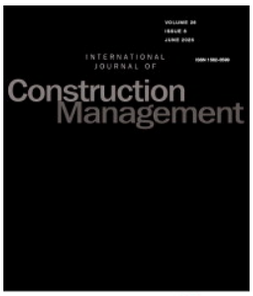

International Journal of Construction Management

ISSN: 1562-3599 (Print) 2331-2327 (Online) Journal homepage: www.tandfonline.com/journals/tjcm20

Feasibility of biochar depth insertion using permeation method in sandy soil for carbon sequestration: a multiphase coupled fluid modelling approach

Absam Moosa Ali & Mavinakere Eshwaraiah Raghunandan

To cite this article: Absam Moosa Ali & Mavinakere Eshwaraiah Raghunandan (28 May 2026): Feasibility of biochar depth insertion using permeation method in sandy soil for carbon sequestration: a multiphase coupled fluid modelling approach, International Journal of Construction Management, DOI: 10.1080/15623599.2026.2676830

To link to this article: https://doi.org/10.1080/15623599.2026.2676830

Published online: 28 May 2026.

INTERNATIONAL JOURNAL OF CONSTRUCTION MANAGEMENT
https://doi.org/10.1080/15623599.2026.2676830

Feasibility of biochar depth insertion using permeation method in sandy soil for carbon sequestration: a multiphase coupled fluid modelling approach

Absam Moosa Ali[a] and Mavinakere Eshwaraiah Raghunandan[a,b]

[a]Department of Civil Engineering, School of Engineering, Monash University Malaysia, Bandar Sunway, Selangor Darul Ehsan, Malaysia; [b]Monash Climate-Resilient Infrastructure Research Hub (M-CRInfra), School of Engineering, Monash University Malaysia, Bandar Sunway, Selangor Darul Ehsan, Malaysia

ABSTRACT

Biochar, a by-product of biomass pyrolysis, is increasingly recognized for carbon sequestration; however, its field-scale use remains limited by uncertainties in practical application methods, placement depth, and delivery efficiency. This study addresses this gap by evaluating pressure-driven biochar slurry permeation in sandy soil using a coupled multiphase porous-media CFD framework. The numerical model underwent a two-stage validation process: first, to verify the porous-media setup and analyze the pressure and velocity responses of saturated sand, and next to validate the hydraulic behaviour of biochar-amended sand against the existing literature. Field-scale simulations were then performed to assess factors (injection time, pressure, inlet diameter, biochar concentration, and application depth) affecting slurry spread and biochar retention. Results highlight that increasing injection pressure and inlet diameter enhance plume spread and retention, while higher BC% reduces slurry mobility under the same conditions. Application depth significantly influenced target-zone placement, underscoring the importance of deep biochar insertion in sandy soils. While this study focused on slurry permeation in homogeneous soil, further research on biochar-soil interactions and clogging mechanisms is needed for effective field carbon sequestration. The findings advocate for deep biochar insertion to enhance resource use and carbon sequestration, aligning with UN Sustainable Development Goals 12 and 13.

ARTICLE HISTORY
Received 27 February 2025
Accepted 14 May 2026

KEYWORDS
Decarbonizing building industry; porous media flow; suspension rheology; carbon sequestration; climate action; computational fluid dynamics; sandy soil; permeation; biochar

Introduction

Biochar is a prominent by-product of biomass pyrolysis and has various applications in both industry and agriculture. Biochar typically comes from a wide range of biomass types and stores abundant carbon (up to 60%), featuring fertilizing compounds such as nitrogen and phosphate. Using different concentrations of biochar as a soil amendment is well-known to enhance soil fertility, physicochemical properties, biological properties, and overall soil quality, making biochar-amended soils a preferred method for carbon sequestration (He et al. 2021; Mohamed and Raghunandan 2025) at the shallow depths in plantation and agricultural fields. For example, Lehmann et al. (2006) estimated 5.5–9.5 pentagrams of annual storage carbon, justifying soil biochar amendment as an effective carbon sequestration approach. Beyond its agronomic role, biochar can also be situated within the broader circular-economy transition of the construction sector, where recent scholarship emphasizes industrial symbiosis, waste valorization, and eco-industrial material systems as pathways to reduce raw material consumption and support lower-emission construction practices (Genc et al. 2020; Genc 2021, 2022; Genc and Kurt 2024). In this context, biochar is particularly relevant as a waste-derived carbonaceous material with durable carbon storage potential

CONTACT Mavinakere Eshwaraiah Raghunandan mavinakere.raghunandan@monash.edu

and emerging applicability in low-carbon construction materials and sustainable material systems (Barbhuiya et al. 2024).

Supplementing biochar into the soil changes the properties, ecosystem, biota, and overall feasibility of the biochar-amended soil from a geotechnical engineer's perspective. At a fundamental level, the bulk unit weight of the biochar-amended soil decreases with increasing biochar content (BC%), attributed to the lower specific gravity of the biochar compared to that of soils (Himanshu et al. 2019). The optimum moisture content (OMC) of biochar, as determined using the standard compaction test procedure (ASTM D698-12:2021), increases with BC% across soil types, due to improved water absorption and holding capacity within the biochar's porous structure (Shane R. Brockhoff et al. 2010). In similar lines, biochar amendment of sandy-type soils shows a decrease in saturated hydraulic conductivity (K_{sat}) with increasing BC% (Githinji 2014; Jun Zhang et al. 2016). On the contrary, silty to clayey-type soils show increasing K_{sat} with increasing BC% (Jien and Wang 2013; Bohara et al. 2019; Sun et al. 2020). Overall, the variation in K_{sat} with soil types is mainly attributed to soil porosity and pore structure. Sandy soils typically have well-defined initial pore structures and volume. Supplementing fine biochar particles will likely lead to blockages in the pore structure, increasing the tortuosity of the drainage path. However, the initial pore space is typically smaller than biochar particle sizes in silty or clayey soils. This results in intra-porosity between biochar and soil pores, thus increasing K_{sat}. Most of the studies rely on one range of biochar particles. A few literature, such as by Trifunovic et al. (2018), have extended to a research scenario by varying the biochar particle size. In scenarios involving unsieved biochar, a preliminary increase in K_{sat} was noted for homogeneous sands. This response is related to the lack of fine biochar particles at low BC% values, which are insufficient to clog the pores (Trifunovic et al. 2018). This interpretation is further supported by Chen et al. (2022) whereby it is reported that reduced infiltration in compacted biochar-amended silty sand despite an increase in total pore volume, as the addition of fine biochar particles reduced the proportion of larger pores and altered the pore-size distribution. Recent work by Chen et al. (2023) further suggests that the hydraulic response of biochar-amended soils is not static, as freeze–thaw-induced microstructural rearrangement and micro-crack formation can substantially alter saturated permeability over time. Recent studies further suggest that this hydraulic response is governed not only by total porosity, but also by effective pore connectivity and wettability, as biochar can modify connected macropores, contact angle, and flow stability within the soil matrix (Liu et al. 2022; Jia et al. 2024). These discussions indicate that the size of biochar particles, soil composition, BC%, pore connectivity, and wettability can collectively affect the K_{sat} values of biochar-amended soil along with environmental conditions the soil is subjected to.

While biochar has been proven to be able to manipulate soil properties, its application in the experimental setup does not represent real-field application conditions. Most laboratory studies involve preparing biochar-amended soil samples using the hand-mixing approach. Biochar application, often achieved by hand mixing with fertilizers and manure, is a common practice in the field and is not limited to laboratory studies. However, this approach is costly and labour-intensive (El-Naggar et al. 2019). In addition, existing field application methods are primarily designed for surface broadcasting, shallow incorporation, spot placement, banding, or deep banding, rather than controlled subsurface placement at depth, making them inherently more suitable for shallow amendment than targeted deep insertion (Major 2010; Brown et al. 2023). Verheijen et al. (2010) further noted that the top-soil application methods may result in biochar particle erosion due to disparities in densities between sand and biochar particles, suggesting depth application to improve soil quality. This concern is consistent with more recent assessments showing that fine biochar particles are more susceptible to detachment and transport near the soil surface (Sharma et al. 2025). Moreover, the practical deployment of biochar at field scale is constrained not only by labour demand, but also by transport, handling, and application logistics, as the low bulk density of biochar complicates field delivery and broader economic reviews show that deployment costs remain highly case-specific and can hinder adoption (Campion et al. 2023; Ibitoye et al. 2024). Therefore, while conventional mixing approaches may be appropriate for shallow sequestration, they remain impractical for controlled deep placement evidenced with a multitude of issues with retention capabilities and erosion. Current methods do not provide an efficient means of inserting biochar into deeper permeable soil layers in a targeted manner. This study therefore proposes

the permeation method to address this gap by transporting biochar as a slurry through the soil pore network under a pressure gradient, thereby avoiding bulk soil mixing and offering a more practical pathway for deeper subsurface insertion. The ability of permeation grouting to replace void fluids with cement grout without altering the soil structure makes it a highly viable method for soil stabilization (Celik 2019). Additionally, in comparison to existing biochar amendment methods, permeation grouting can be less labour intensive and cost friendly. The grout used in the cement grouting method usually consists of a cement slurry. Having said that, can cement be replaced with biochar as the permeate? Though the purpose of cement and biochar permeation defers, the objective is to fill the soil void space with the permeate. In the case of biochar, this would be an effective depth insertion method for CO_2 sequestration, which is the fundamental motivation and focus of this study.

In exploring an innovative in-field permeation approach, it is therefore essential that the permeate used is a biochar slurry. Biochar in slurry form would be ideal as it eases the permeation method, and the biochar would remain suspended in the slurry due to its hydrophobic behaviour (Edeh and Mašek 2022). Assessing the flow behaviour of biochar slurry, in addition to the properties of biochar-amended soil, is crucial for ensuring the efficiency of biochar permeation through the soil. However, clogging pore spaces is a critical process affecting the efficiency of slurry (prepared using suspended hydrophobic material like biochar) permeation through porous media (Githinji 2014). Though studies using biochar slurry mixes show a more profound effect on soil properties (Abdo 2021), no existing experimental research has considered using biochar and water mixtures (or biochar slurry). Viewing biochar slurry as a liquid with suspended particles enables better control over biochar sequestration by establishing a relationship between solid content (rheological behaviour), viscosity, biochar particle size, and flow properties (Liu et al. 2017). The main aim of this study is to evaluate the suitability of biochar slurry permeation through compacted sandy soil layers as an effective in-field depth injection of biochar using a combination of laboratory-scale experimental modelling and computational fluid dynamics-enabled finite element modelling.

Literature has explored the effects of biochar on reducing water infiltration and increasing soil stability through finite element modelling (Ng et al. 2022). Additionally, biogeochemical modelling has been used to demonstrate the effectiveness of biochar sequestration over time (Yin et al. 2022). Thus, no specific studies have considered the transport of biochar in soil or its use as a soil amendment for carbon sequestration. However, a preliminary attempt by Yin et al. (2022) demonstrates a decrease in K_{sat} over time in sandy clay loam soil. This suggests that numerical modelling can effectively study the feasibility of field-scale implementation of biochar amendment in soil. Due to the limited literature on biochar permeation, numerical simulations related to cement (permeation) grouting in soils serve as valuable references. Multiphase modelling using computational fluid dynamics (CFD) effectively simulates cement grouting in saturated soil while accounting for heat transfer within the soil medium (Zhelnin et al. 2020). Zhou et al. (2021) illustrated replacing water-filled porous zones with grout and forming a grout-water mixture, referred to as transition zones before complete water displacement occurs. However, these analyses did not consider clogging effects, which may lead to an inaccurate representation of how suspensions such as grout affect soil porosity and permeability through the soil layer. Li et al. (2022) introduced a numerical solution for grouting in saturated soils, integrating the volume-of-fluid (VoF) method with the discrete element method (DEM). In the study by Li et al. (2022), particle interactions are governed by Newton's laws of motion, utilizing a no-slip model for these interactions. Moreover, using VoF allowed the modelling of two immiscible liquids, with separate volume fractions used for water and grout phases. Using multiphase models like VoF combined with CFD that incorporate porous media flow may provide an effective method for simulating the field-scale infiltration of biochar into the soil.

Most previous studies on biochar-amended soils have focused on uniformly mixed biochar and the resulting changes in hydraulic and geotechnical properties. Although such studies are useful for understanding amendment effects, they do not represent the practical challenge of targeted deep biochar insertion in the field. Existing work on biochar slurry is also limited in explaining its transport and deposition behaviour within porous soils, while numerical studies of porous media generally do not address biochar-specific permeation using a validated coupled framework. Therefore, the present study advances the

literature by investigating pressure-driven biochar slurry permeation in sandy soil as a potential deep-insertion strategy. Due to the lack of literature available for such a numerical modelling scenario, the study first incorporates a validation stage where water is allowed to infiltrate freely into soil to investigate whether CFD models can properly represent the pressure and velocity behaviours expected in soil porous mediums. The second stage involves the base porous-medium representation of the sandy soil which is validated against hydraulic behaviour, particularly permeability response, to establish the governing soil resistance parameters. The numerical framework coupled slurry flow behaviour with porous-media transport, allowing the interaction between biochar suspension properties and soil hydraulic resistance to be resolved more explicitly before extending the analysis to field-scale implementation.

Materials and methods

Assumptions for numerical simulation

Understanding various considerations and assumptions when developing a numerical model is an essential step in ensuring the repeatability and suitability of the numerical model. The following assumptions serve as the basis for the modelling scenario considered in this study. The assumptions justify the approach and framework used to define porous media and how biochar acts in the medium.

1. The soil layer is represented as a rigid porous medium composed of compacted coarse sand with homogeneous and isotropic properties. The soil skeleton is assumed immobile during injection, and local heterogeneity, preferential flow paths, and particle-scale variability are neglected.
2. The porous medium is assumed to be fully saturated throughout the permeation stage. Entrapped air, partial saturation, and capillary effects are not considered as the analysis focuses on slurry transport through water-filled pore spaces.
3. Hydraulic response of the sand to the permeation of slurry is defined by its initial effective pore structure. Any progressive reduction in flow capacity caused by retained biochar is represented at the continuum scale through effective permeability changes rather than resolving pore-scale bridging.
4. Biochar is introduced as a particulate suspension in water rather than as a separate immiscible liquid phase. While the sand is treated as a stationary porous matrix, the slurry is represented through the bulk properties of the injected slurry.
5. The injected biochar slurry is modelled using effective bulk properties corresponding to the selected slurry condition. The solid content present in biochar is quantified by weight percentage with an effective density and viscosity values.
6. The rheological behaviour of the biochar slurry is represented using literature-derived apparent viscosity values rather than pure-water properties. Liu et al. (2017) showed that biochar-water slurries exhibit concentration-dependent, particle-size-dependent, and shear-thinning behaviour, with viscosity and yield stress also influenced by water uptake into the internal pores of biochar particles. In the present model, this behaviour is simplified by assigning an effective apparent viscosity for the selected slurry condition.
7. The internal pore structure of individual biochar particles is not resolved explicitly. Open and closed intra-particle pores are therefore not modelled separately. Their net influence is assumed to be embedded within the effective bulk slurry properties adopted from the literature, including density and viscosity. This simplification avoids particle-scale modelling but may affect the absolute prediction of flow behaviour.
8. The injected slurry is assumed to remain uniformly mixed during the modelled injection period. Particle settling, segregation, aggregation, breakage, dissolution, and chemical interaction with pore water are neglected unless otherwise stated.
9. Flow is assumed incompressible and isothermal. Thermal effects, compressibility, and physicochemical reactions between biochar and the soil matrix are not considered.

Computational fluid dynamics (CFD) multiphase model

The general-purpose CFD software ANSYS Fluent 2021 R1 is utilized in this study to simulate the movement of biochar permeate through the model soil bed. The porous media flow equations were coupled with multiphase models to represent the behaviour of biochar slurry insertion into the model soil bed. The possible influence of non-Darcy flow was also assessed in this study. Unlike leakage-induced erosion problems, where local defect outflow and particle loss may cause elevated seepage velocities and inertial effects, the present study considers pressure-driven permeation through an intact saturated compacted sand layer. Based on the representative sand grain size, porosity, and effective slurry viscosity used in the model, the estimated pore-scale Reynolds number remained well below unity under the applied pressure range. This indicates that the flow remained within the Darcy regime, and viscous resistance was dominant. Therefore, inertial losses were neglected, and Darcy-based porous media resistance was considered sufficient for the present simulations.

The Euler–Euler approach was considered appropriate because it allows each phase to be represented in a continuum sense through a set of governing equations allowing for effective simulation of geotechnical problems involving multiple physics while avoiding the numerical instabilities which come along with the scale of the simulation (Evans et al. 2016). In the present study, the soil sample is assumed to be fully saturated and the influence of air is neglected, such that the model focuses on the interaction of biochar slurry with water-filled soil pores. At the continuum scale adopted in this study, the injected permeate is treated as a water-based suspension of fine biochar particles moving through a saturated porous medium, rather than as a system containing a sharp fluid–fluid interface. In addition, the homogeneous treatment was considered acceptable because the objective of the present model is to capture the average pressure-driven permeation response of a fine biochar-water suspension through the saturated porous medium at the continuum scale, whereas particle-scale segregation, collision, and deposition effects were treated as secondary processes beyond the scope of the adopted formulation. Liu et al. (2017) showed that biochar-water slurry behaves as a flocculated suspension with concentration-dependent viscosity and shear-thinning behaviour, while water uptake into the internal pores of biochar particles further affects its apparent bulk behaviour. Since the main objective of this study is to evaluate the overall permeation behaviour of the slurry through the porous soil layer rather than the motion of individual particles, the slurry was approximated using effective bulk mixture properties, and a homogeneous mixture treatment was considered appropriate.

ANSYS Fluent includes several homogeneous models, such as the VoF model, Mixture model, and Eulerian model. As the present study incorporates permeate interaction with soil pores at a continuum scale rather than sharp fluid to fluid interfaces, the mixture model is the most suitable choice from the available multiphase models. According to ANSYS (2009), the mixture model is suitable for two or more phases treated as interpenetrating continua, and it may be used either for phases moving at different velocities under local equilibrium over short spatial scales or for homogeneous multiphase flow when the phases are strongly coupled and move at the same velocity. The model solves a single mixture momentum equation and uses volume fraction equations for the secondary phases, which makes it suitable for particulate suspensions represented through average bulk transport behaviour. In contrast, the VoF model is intended for immiscible fluids where the location of a distinct interface must be tracked, while the full Eulerian model solves separate momentum and continuity equations for each phase and therefore requires additional interphase closures and significantly greater computational effort. For the present problem, where the objective is to capture the overall permeation behaviour of biochar slurry through porous soil rather than particle-scale segregation or collision mechanics, the mixture model was considered the most appropriate balance between physical representation and computational tractability. This choice should be interpreted as a continuum-scale approximation of average slurry permeation, since the adopted mixture formulation does not directly resolve particle-size-specific transport, transient concentration redistribution, or pore-scale deposition and clogging development. These effects were not resolved explicitly because the present study aims to capture the average continuum-scale permeation response of biochar slurry through the saturated porous medium, rather than particle-scale transport and deposition mechanisms. A more detailed treatment of particle-size-specific transport,

concentration evolution, and transient clogging would require additional closure relationships or CFD–DEM type coupling beyond the scope of the present model and the objectives of this study.

Governing equations

The mixture model typically functions by solving the continuity and momentum equations for the mixture, together with volume fraction equations for the secondary phases and algebraic expressions for relative velocity when slip between phases is considered. The numerical assessment involves a coupled approach integrating multiphase flow with porous media flow. The porous media model in ANSYS Fluent uses a superficial velocity formulation in which the effect of the porous medium is introduced as a momentum sink, thereby accounting for pressure loss through the porous region under either transient or steady-state conditions (ANSYS 2009). In ANSYS Fluent, porous-media flow is represented through a source term added to the momentum equations, where the source term accounts for viscous resistance and, when required, inertial resistance within the porous zone. Equation 1 defines a combination of a source term (S_i) and a fluid flow equation to calculate the pressure drop caused by fluid flow. This equation describes terms C and D as prescribed matrices, while υ represents the fluid velocity. The variable μ denotes the viscosity of the penetrating fluid, and ρ defines the density of the penetrating fluid which is the biochar slurry in this case. The equation can be separated into individual directions, such as x, y, or z, represented in the equation as '*i*'.

$$S_i = -\left(\sum_{j=1}^{3} D_{ij}\mu v_j + \sum_{j=1}^{3} C_{ij}\frac{1}{2}\rho|v|v_j\right) \tag{1}$$

Equation 1, in terms of a homogeneous media by introducing permeability, results in Equation 2, C_2 and $\frac{1}{K}$ is introduced as a result of specifying C and D as diagonal matrices.

$$S_i = -\left(\frac{\mu}{K}v_i + C_2\frac{1}{2}\ \rho|v|v_i\right) \tag{2}$$

For the present study, Equation (2) was applied in each coordinate direction under the pressure-based laminar solver. Since the estimated pore-scale Reynolds number remained well below non-Darcy flow considerations for all simulated conditions, the inertial resistance term was neglected by setting $C_2 = 0$, such that the pressure drop in the porous medium remained proportional to velocity and Darcy based resistance was considered sufficient. The multiphase model includes the continuity equation, as shown in Equation 3, representing the conservation of mass for the mixture.

$$\frac{\partial}{\partial t}(\rho_m) + \nabla \cdot (\rho_m \vartheta_m) = 0 \tag{3}$$

where ρ_m is defined as the density of the mixture and ϑ_m is the mass-averaged velocity of the porous medium over time. In the present formulation, these governing equations are used to represent the average continuum-scale permeation behavior of biochar slurry through the saturated porous medium, while particle-size-specific transport, transient concentration redistribution, and pore-scale deposition are not resolved explicitly.

Model setup

Figure 1 illustrates the procedure used in the two-stage validation process employed in this study. The first stage involves modelling the soil layers using similar simulation methods described in the literature (Alam et al. 2020; Diana et al. 2021). The main focus of this stage was to confirm that the numerical simulation could accurately model the response and behaviour simulating flow through soil (a typical porous media). To achieve this, the simulation procedure employed a porous soil medium that was subjected solely to water flow. This step was essential to ensure that the soil medium exhibited behaviour typical to a flow through porous media as reported in the literature (Alam et al. 2020; Diana et al. 2021). At this stage, the formation of pressure contours due to an increase or decrease in static pressure

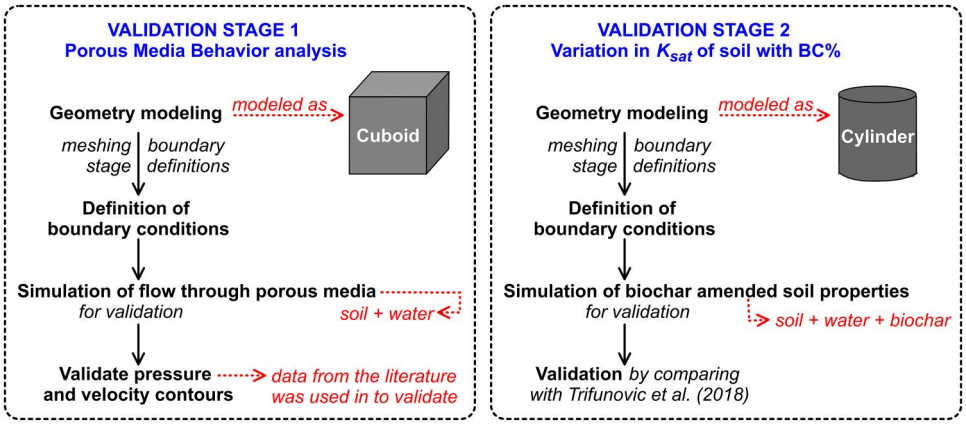

Figure 1. Schematic diagram showing the two-stage validation process adopted in this study.

in the porous medium due to water flow and the input boundary conditions were simulated for different conditions. This approach of developing pressure contours is also useful and essential in simulating multiphase flow in porous media (Alam et al. 2020; Diana et al. 2021).

The second stage of validation was conducted to evaluate the hydraulic response of biochar-amended sand, since this material constitutes the actual porous medium considered in the present study. The experimental data of Trifunovic et al. (2018) were selected as the primary validation dataset because they are directly relevant to the present work in terms of sandy soil conditions and the influence of biochar particle size. Their experiments used a homogeneous Ottawa sand medium (ASTM 20–30 sand) with d_{10}, d_{50}, and d_{90} values of 0.67, 0.90, and 1.24 mm, respectively, which is particularly suitable for defining the porous-medium properties in the present model. K_{sat} was measured using a bench-top UMS KSAT device based on the falling-head method and Darcy's equation; however, no formal ASTM or ISO hydraulic testing standard was explicitly reported. Accordingly, the second-stage validation reproduced the falling-head permeability response of the biochar-amended sand and compared the simulated K_{sat} trends with the experimental results reported by Trifunovic et al. (2018), particularly for the unsieved and fine biochar cases. The flowrate at the outlet of the soil sample was extracted and plugged into the following Equation 4 to obtain the simulated K_{sat} value.

$$K_{sat_{simulated}} = \frac{Q \cdot L}{A \cdot \Delta h} \tag{4}$$

where Q is the flowrate at the outlet of the soil sample simulation, L is the length of the sample, A being the surface area of the soil, and Δh is the pressure change induced by the permeability test. This stage was used to confirm that the selected model parameters and numerical procedure could adequately represent the hydraulic behavior of biochar-amended sand prior to the subsequent permeation analysis.

Agreement with literature data was evaluated using pointwise relative error and overall trend consistency. The relative error for each data point was calculated and the overall discrepancy for each dataset was assessed from the average of these pointwise errors. In addition to the numerical error, the model was required to reproduce the characteristic response shape reported in the experimental study, such as monotonic reduction in K_{sat} or non-monotonic threshold behavior with increasing biochar content. In the present study, validation was considered acceptable when the overall error remained below 10% and the experimental trend was reproduced correctly.

Upon completion of the validation stage, simulations of biochar permeation were performed on the test soil samples by systematically varying the model parameters. Figure 2 presents a flow diagram highlighting the essential numerical processes and analyses used in this study. This stage primarily concentrated on evaluating and monitoring the distribution of biochar in the soil. The assessments were conducted considering the volume fraction of water and/or biochar present within the medium, at a spatial scale. The parametric study involved several variables, including injection time, injection pressure, biochar concentrations, the diameter of the permeation inlet, and the depth of biochar

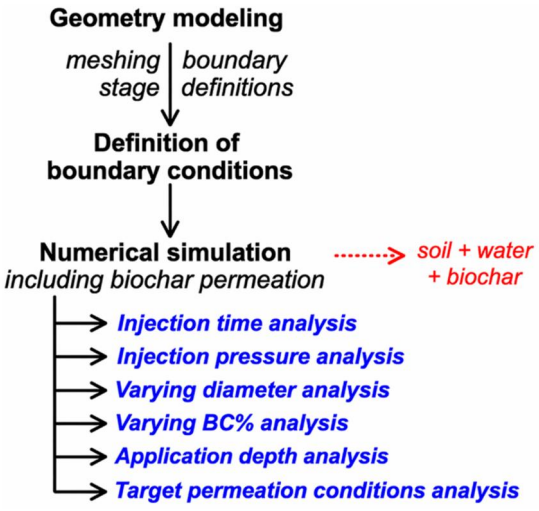

Figure 2. Flow diagram highlighting the key numerical processes and analyses adopted.

application. Injection time sensitivity was assessed from 300 to 2100s at 300 s intervals. This range was chosen to cover short, intermediate, and extended injection durations under pressure-driven permeation, while the fixed interval allowed systematic identification of time-dependent changes in plume spread and retained mass. To further evaluate post-injection behaviour, a second analysis was performed in which injection was stopped at 1500s by changing the inlet boundary to a wall. The subsequent settling response was first examined over additional durations of 0 to 900 s after shutoff, and because only minor changes were observed, a longer settling period of 3600s was included to assess the 1 h stabilization behaviour of the permeated slurry. Injection pressure was varied from 10 to 200 kPa for 600 s to examine the effect of progressively increasing pressure gradients on biochar slurry permeation. This range was chosen to cover low to moderately elevated pressures while remaining focused on permeation in sandy soil, since grouting pressure is known to govern whether slurry diffusion occurs mainly by permeation or shifts toward compaction or fracture at higher pressures (Hu et al. 2024). Therefore, the selected pressures were considered sufficiently high to produce measurable permeation response, but low enough to avoid moving the analysis away from the intended permeation regime (Zhong et al. 2023). Injection diameter was varied from 0.1 to 0.5 m to represent realistic field-scale inlet or augured opening sizes. Commercial hydraulic auger systems commonly provide drilling diameters within this range, including standard sizes from 100 to 500 mm, which supports the practical relevance of the selected values (Auger Torque, 2023n.d.). The range also allowed the effect of increasingly larger injection footprints on slurry permeation behaviour to be assessed systematically. Biochar content was varied from 25 to 40 wt% based on the rheological data reported by Liu et al. (2017), since these were the values that could be extracted directly and consistently for use in the present model. This range was selected because it represents relatively high-solid slurry conditions, which are more relevant for evaluating biochar delivery and retention in soil than highly dilute mixtures. Using this range also avoids overly dilute slurry cases, which would introduce more water relative to biochar and would be less representative of a practical sequestration-oriented permeation approach. At the same time, it allows the influence of progressively increasing solids concentration on slurry viscosity and permeation behaviour to be assessed in a systematic manner. The application depth was varied based on the constant injection diameter used in this part of the study ($d = 0.3$ m), using depths of $3d$, $6d$, $9d$, $12d$, and $15d$. This was done so that the depth could be defined relative to the size of the injection region, rather than selecting arbitrary absolute values. Using normalized depths in terms of diameter also makes the comparison more consistent, since each case represents a progressively deeper placement condition under the same inlet geometry. The extent of slurry permeation was quantified from the slurry volume fraction (VF) distribution. The core plume was defined as the region where VF > 0.5; thus, core vertical spread and core horizontal spread represent the depth and lateral width of this main concentrated zone. The overall permeation

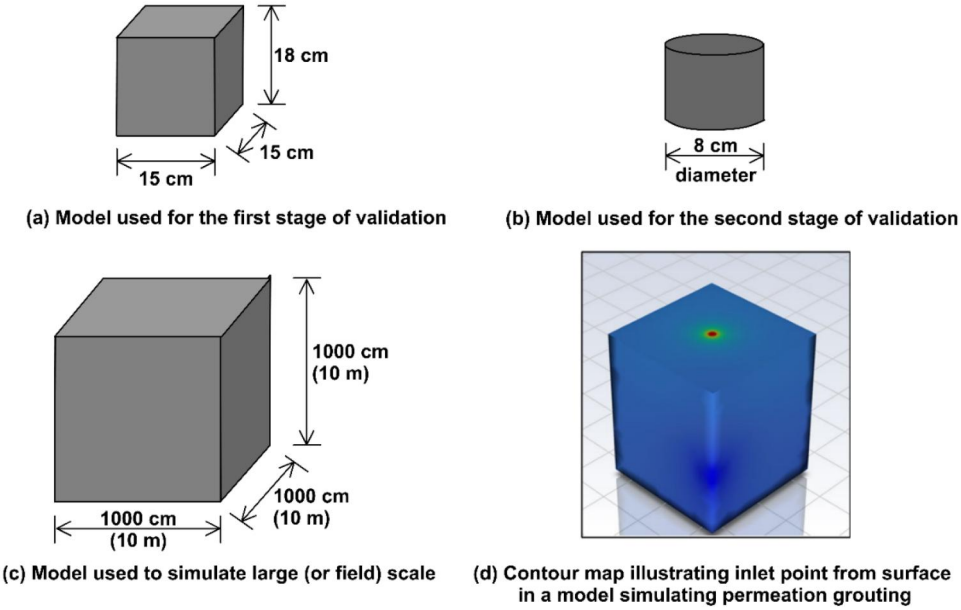

Figure 3. Geometry and dimensions of all soil models used throughout the analysis in this study (*note: the figures are illustrative only and not to scale*).

extent was evaluated using a cutoff criterion of VF < 0.05, where total vertical spread represents the maximum downward penetration depth and max lateral spread represents the furthest horizontal reach of the slurry. Retained slurry mass denotes the total slurry remaining in the soil domain, whereas retained biochar mass denotes the retained solid biochar fraction. Following the sensitivity analyses, a target-depth screening procedure was used to identify feasible design cases. The predicted downward spread (L_{pred}), maximum lateral spread (W_{pred}), and retained biochar mass $(M_{b,pred})$ were estimated from the corresponding reference values $(L_{ref}, W_{ref}, M_{b,pred})$ using multiplicative factors $(F_P, F_L, F_D, F_{BC}, F_A)$ derived from the pressure, diameter, biochar-content, and application-depth analyses as seen in Equations 5, 6 and 7.

$$L_{pred} = L_{ref} F_{P,L} F_{D,L} F_{BC,L} F_{A,L} \tag{5}$$

$$W_{pred} = L_{ref} F_{P,W} F_{D,W} F_{BC,W} F_{A,W} \tag{6}$$

$$M_{b,pred} = M_{b,ref} F_{P,M} F_{D,M} F_{BC,M} F_{A,M} \tag{7}$$

The predicted achieved depth was then calculated as:

$$z_{ach} = z_{app} + L_{pred}$$

A case was considered feasible when $z_{ach} \geq z_{target}$. The feasible cases were then ranked using a screening score defined as:

$$S = \frac{M_{b,pred}}{W_{pred}}$$

where higher values indicate greater retained biochar mass per unit lateral spread. This procedure was used so that the selected best design case reflects practical injection efficiency rather than simply maximum plume extent.

Model geometry and meshing

Figures 3a–c show the three primary model geometries and scenarios used during both the validation and simulation phases of this study. In the initial validation stage, cuboidal-shaped small-scale models, as shown in Figure 3a, were used to represent a typical porous medium and evaluate its response to steady-state flow through this medium. In the second stage of validation, a small-scale cylindrical block was modelled to replicate the experimental specimen used by Trifunovic et al. (2018) during their

testing, as shown in Figure 3b. The numerical simulations were conducted on larger-scale soil blocks, as shown in Figure 3c, to evaluate the effect of biochar permeation at a field scale. A 10 m × 10 m × 10 m cubic domain was adopted as an idealized field-scale subdomain for evaluating pressure-driven biochar slurry permeation. This size was selected to provide sufficient space for plume development and pressure dissipation during the simulated injection period, thereby limiting artificial boundary effects. Preliminary simulations confirmed that the permeation front remained well within the model boundaries for the tested cases, supporting the adequacy of the selected domain dimensions. At the same time, the adopted size remains computationally manageable for the planned parametric analyses. Accordingly, the domain should be interpreted as a representative control volume for field-scale assessment rather than the full extent of an actual site.

Mesh sensitivity checks were conducted for the second validation stage and the field-scale simulations. No mesh sensitivity assessment was performed for the first validation stage, as it was used only to verify that the porous-media inputs in ANSYS Fluent generated the expected pressure and velocity contours. For the second validation stage, mesh sizes from 10 mm to 1 mm were examined. Mesh independence was assumed when the change in results was below 0.5%. Refinement from 5 mm to 2.5 mm changed the results by 0.1%, while further refinement to 1 mm changed the results by 0.3%. Accordingly, a mesh size of 2.5 mm was adopted for the validation stage to balance accuracy and computational efficiency.

A mesh sensitivity analysis was carried out for the field-scale model using mesh sizes of 0.20, 0.15, and 0.10 m for the representative case of 25 kPa injection pressure, 25% biochar content, 0.3 m injection diameter, and 600 s injection time. The predicted core vertical spread, core horizontal spread, and retained biochar mass were used to assess mesh independence. Refinement from 0.20 to 0.15 m changed these quantities by 0.85%, 0.73%, and 0.35%, respectively, whereas further refinement from 0.15 to 0.10 m changed them by 1.07%, 0.82%, and 0.35%, respectively. As the variations remained small, a mesh size of 0.15 m was selected for the field-scale analyses to balance accuracy and computational efficiency.

This study is controlled by two key geometric parameters: the diameter and depth of biochar insertion. The inlet point, where biochar flows into the soil medium, is, therefore, a crucial aspect of the model's geometry as it essentially controls the flowrate of slurry into soil. The inlet point is modelled by defining a diameter at the midpoint of the soil surface, as shown in Figure 3d. The flow into the soil depends on volumetric flow, which considers both velocity and the area of permeation. A diameter analysis was also conducted as part of a parametric study, which included of gradually increasing the diameter while maintaining a fixing all other parameters. Another essential aspect of the numerical simulation in this study is the depth of biochar application. This parametric simulation aims to investigate how increasing the depth of biochar application into the soil affects its overall distribution within a typical soil medium. To enable this simulation, the original inlet point shown in Figure 3d was established at various depths beneath the surface through extrusion. The non-geometric variables assessed in this study include the injection time of slurry, the injection pressure of the permeate and, the BC% of the slurry. These parameters mostly affect the flow properties of slurry in the soil.

Model initialization

The model initialization section focuses on defining the modelling approach in relation to the expected response. In this study, a pressure-based solver is preferred because the permeability of porous media can be characterized by changes in pressure within the soil layer of interest. A steady-state approach was used for the Trifunovic validation because this stage was intended to reproduce the saturated hydraulic conductivity of the biochar-amended sand, not the transient falling-head process itself. Although Trifunovic et al. (2018) obtained K_{sat} using a falling-head method, the reported validation target is the final conductivity derived from Darcy's equation rather than the full time-dependent head response. Therefore, steady-state flow through the saturated amended sample was considered adequate for validating the hydraulic property of the porous medium, whereas transient analysis was reserved for the finite-duration biochar slurry permeation simulations. As such, transient analysis was selected for the field scale scenario as the objective of the study was not to determine a final equilibrium flow state,

Table 1. Biochar slurry properties adopted for the study.

Biochar loading (BC %)	Viscosity (kg/ms)	Density (kg/m^3)
25	0.15	530.1
30	0.28	484.6
35	0.58	446.2
40	0.98	413.5

but to simulate the progressive permeation of biochar slurry during finite-duration injection. Since plume development, pressure dissipation, and slurry retention all evolve with time, a steady-state approach would not be able to capture the temporal response needed for validation and field-scale comparison. Gravity was also included as part of the model with a defined acceleration downwards of 9.81 m/s^2.

Material properties

Among the studies reviewed, Liu et al. (2017) was the only paper identified that systematically reported the rheological behaviour and stability of biochar-water slurry over a range of biochar loadings and particle sizes, making it the most suitable source for defining slurry properties in the present model. The viscosity values used in this study were taken from Figure 6, specifically from the unimodal fine-biochar case with $D_{50} = 2.2$ μm, evaluated at a shear rate of 100 s^{-1}. This graph was selected because the present work focuses on permeation through a porous sand medium, where the injected slurry is intended to behave as a fine suspended phase capable of entering pore spaces rather than as a coarse slurry dominated by settling and segregation. This choice is also supported by Liu et al.'s observation that finer biochar produced more stable slurry systems and showed lower sedimentation tendency, which is more consistent with the intended injection and permeation conditions considered in this study. The corresponding apparent viscosities at 25, 30, 35, and 40 wt.% biochar loading were therefore extracted from that curve and used as the effective slurry viscosities in the model.

For density, the same biochar type reported by Liu et al. (2017) was adopted as the reference material. Their slurry was prepared using pine sawdust biochar produced by pyrolysis at 750 °C in the absence of air. Because Liu et al. focused on rheological behaviour and did not explicitly report a bulk density value for the dry biochar, the slurry density in the present study was estimated on the basis of the reported biochar loading by weight, using the Liu et al. biochar type as the reference material and treating the resulting slurry as an effective bulk mixture. Thus, the density values used in the model should be interpreted as effective slurry densities consistent with the Liu et al. biochar–water system, rather than as particle-resolved densities that explicitly account for the open and closed internal pores of individual biochar particles. Table 1 highlights the properties of biochar slurry adopted for the study. Biochar material properties were not considered for both validation stages, as each stage considered the flow of water into base soil and biochar amended soil respectively and therefore, the soil-biochar characteristics in the second validation stage were solely based on the absolute permeability and porosity of the soil subjected to amendment.

ANSYS Fluent defines viscous resistance as the inverse of absolute permeability, measured in units of m^{-2}. Further analysis indicates that calculating the inverse intrinsic permeability of a soil medium provides this value. Consequently, the permeability (κ) can be expressed as a function of geometry and pore structure, as shown in Equation 8 (James et al. 1999)

$$\kappa = \frac{K_{sat}\mu}{\rho g} \tag{8}$$

This will enable the comparison between the experimental setup and the numerical scenario being modelled. In this case, μ and ρ represent the viscosity and bulk density of the relevant permeate, which is water. Throughout the validation stage, Trifunovic et al. (2018) 's K_{sat} values were consequently converted into the absolute permeability before the inverse value is input as the viscous resistance. As the field-scale study expands the same soil into a slurry permeation scenario, the control 0% BC value was

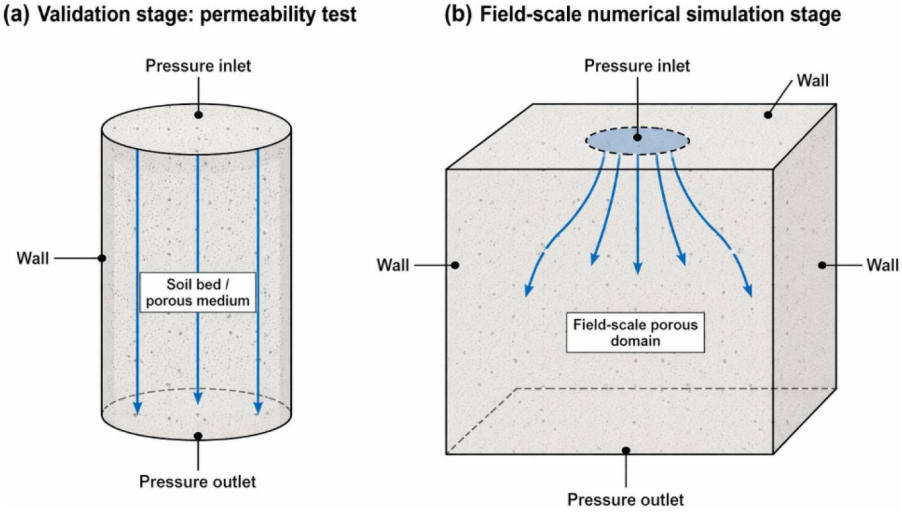

Figure 4. Boundary conditions of all soil models used throughout the analysis in this study (*note: the figures are illustrative only and not to scale*).

input as the absolute permeability value. The corresponding porosity values for each stage were also input based on the available literature values.

Boundary conditions

For the validation-stage simulations as seen in Figure 4a, the top boundary was specified as a pressure inlet and the bottom boundary as a pressure outlet, while the lateral boundaries were modelled as walls. The pressure inlet condition was selected because the imposed hydraulic loading in the validation configuration is pressure-controlled, whereas the corresponding inflow rate is not known a priori; in ANSYS Fluent, pressure inlet boundaries are used precisely for cases in which the inlet pressure is prescribed but the resulting velocity or flow rate is part of the solution (ANSYS 2009). The bottom surface was assigned as a pressure outlet to prescribe the downstream static pressure and allow the fluid to leave the domain under the applied pressure gradient, which is consistent with the falling-head/permeability-type hydraulic response reproduced in this stage. The side boundaries were modelled as walls to represent the rigid and laterally impermeable confinement of the laboratory soil bed, thereby preventing artificial side leakage and restricting flow to the intended vertical permeation direction. In ANSYS Fluent, wall boundaries impose a solid no-slip boundary and are commonly used to represent impermeable confining surfaces. The use of pressure inlet and pressure outlet boundaries for pressure-driven slurry transport in saturated sand is also consistent with previous ANSYS-based grouting simulations (Li et al. 2022).

For the field-scale simulations as seen in Figure 4b, the injection patch at the top surface was specified as a pressure inlet, whereas the remaining top surface and all lateral surfaces were modelled as walls; the bottom boundary was assigned as a pressure outlet. The pressure inlet was used because the field-scale analysis examines pressure-driven injection, for which the applied injection pressure is prescribed and the resulting inflow rate is solved as part of the permeation response. The non-inlet portion of the top surface was treated as a wall so that flow could enter only through the intended injection region, thereby avoiding artificial surface inflow or outflow outside the injector footprint. The side boundaries were also set as walls to represent an idealized confined field-scale subdomain and to prevent lateral leakage through the model limits during the simulated injection period. This treatment is justified because the domain was selected sufficiently large that the permeation front remained within the interior region of the model, so the outer boundaries acted as far-field limits rather than controlling the predicted slurry spread. The bottom surface was defined as a pressure outlet to provide a hydraulic release boundary for displaced pore fluid and to represent continued hydraulic communication below the modelled subdomain under the imposed pressure gradient. As in the validation configuration, the wall boundaries represent impermeable solid limits in Fluent and were used to maintain the intended flow confinement in the modelled field-scale block.

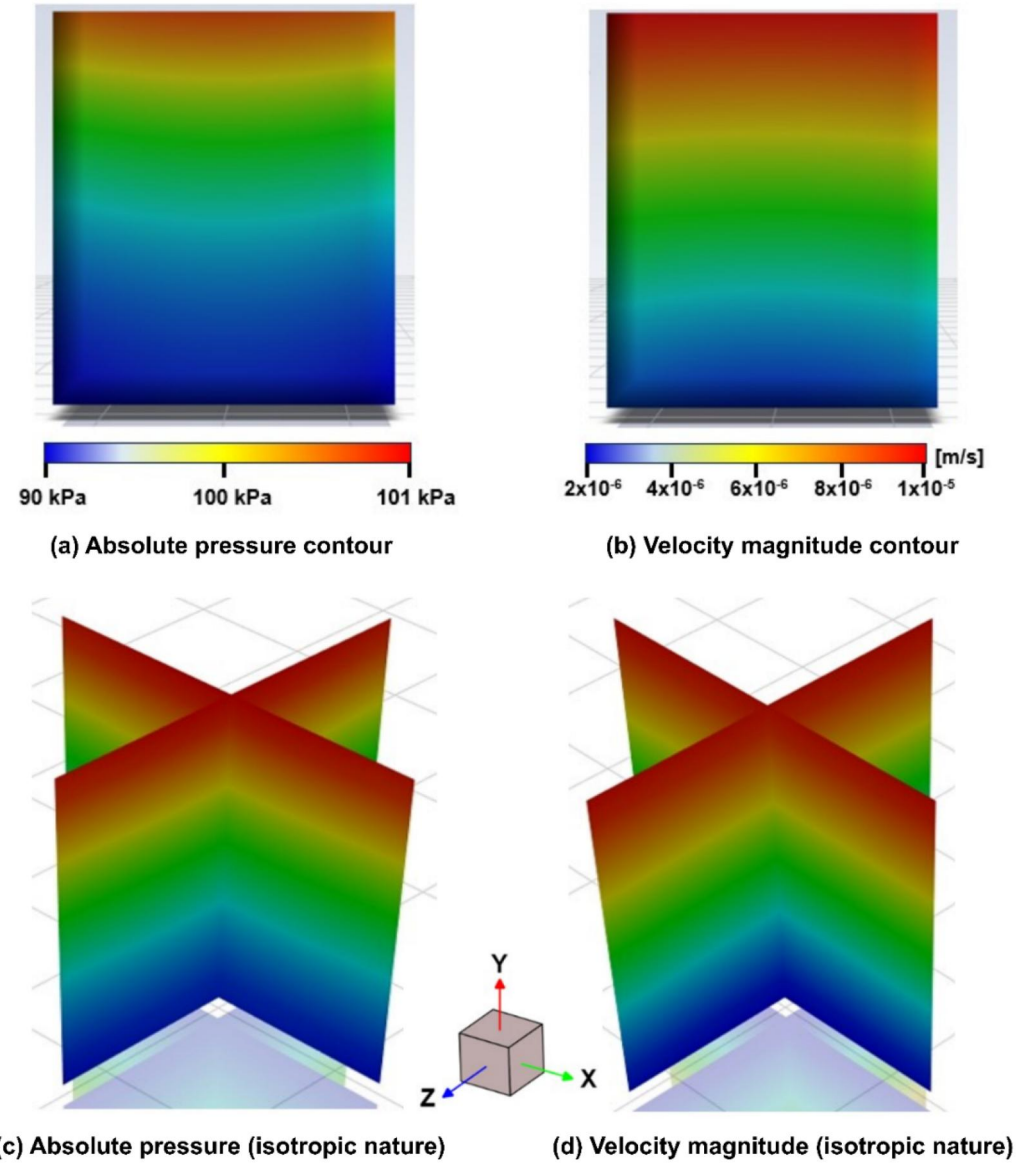

Figure 5. Simulation output from the first stage of validation.

Results

Validation stage 1: Porous media behaviour assessment

The first stage of validation was conducted to verify that the porous-medium model reproduced the expected steady-state hydraulic behaviour. As shown in Figure 5a, the converged solution produced a stable absolute pressure contour, with an overall pressure variation of approximately 1100 Pa across the soil domain. The pressure decreased progressively through the porous medium, and this trend was accompanied by the velocity distribution shown in Figure 4b. The observed response confirms that the assigned porous-medium properties and boundary conditions generated the expected pressure-loss behaviour for laminar flow through the saturated soil layer. It is important to note that the isotropic nature of the medium was confirmed by creating plane sections and observing the behaviour at both planes (*planes along the x- and z-axis*). Figures 5c and d demonstrate constant pressure and velocity contours regardless of the model scales, which validates the assumption of isotropic soil. Therefore, the following sections will focus on the *xy*-plane.

The simulations conducted in this study aimed to determine the optimal diameter for the permeation of biochar slurry into the soil. The validation stage was also used to verify and establish if an inlet diameter of 30 mm was appropriate for this application. Different inlet diameters were used during this phase. Inlet

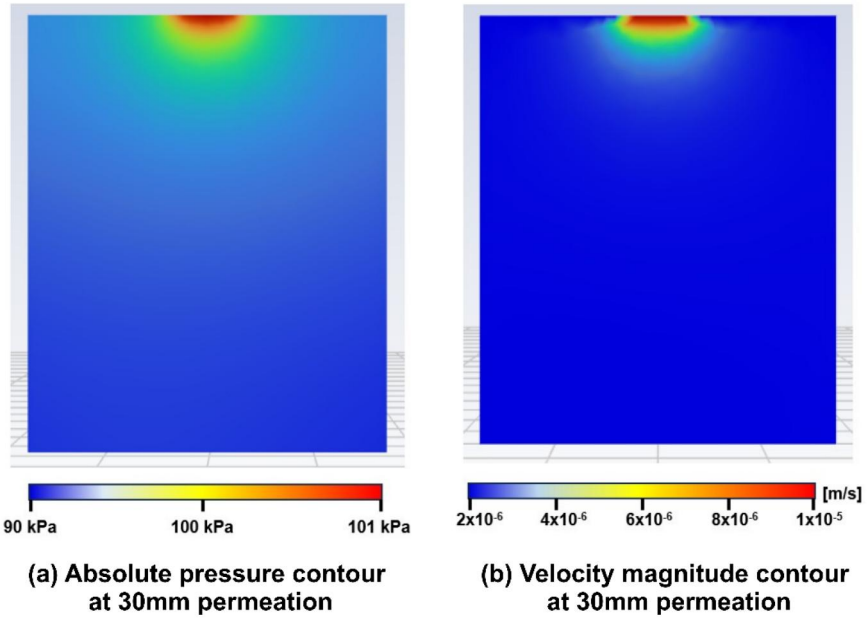

Figure 6. Simulation outcomes for the scenario using a 30 mm permeation inlet diameter.

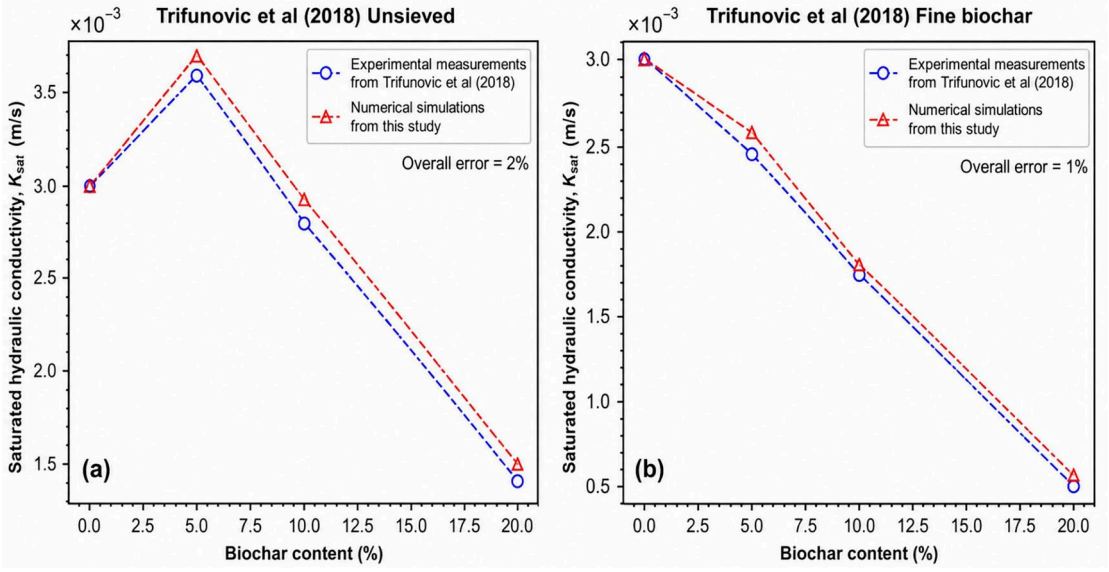

Figure 7. Saturated hydraulic conductivity (K_{sat}) of biochar-amended soil simulated in this study, compared to experimental measurements from the literature where (a) simulated unsieved biochar addition into Ottawa sand and (b) simulated fine biochar addition into Ottawa sand.

diameters smaller than 30 mm generally failed to generate expected pressure and velocity distributions in the soil medium, as the flow rate was contingent upon both the area of the inlet and the initial velocity. In such scenarios, the pressure change within the system was minimal, resulting in insufficient water flow into the soil. Given that water exhibits a relatively low viscosity compared to biochar slurry, it was concluded that these smaller diameters would not facilitate an adequate flow rate necessary to effectively simulate biochar permeation in soil. Figures 6a and b illustrate the pressure and velocity contours resulting from the simulation utilizing a 30 mm diameter inlet. A recorded pressure change of 150 Pa was observed from the pressure contours, which remains low relative to the total area functioning as an inlet.

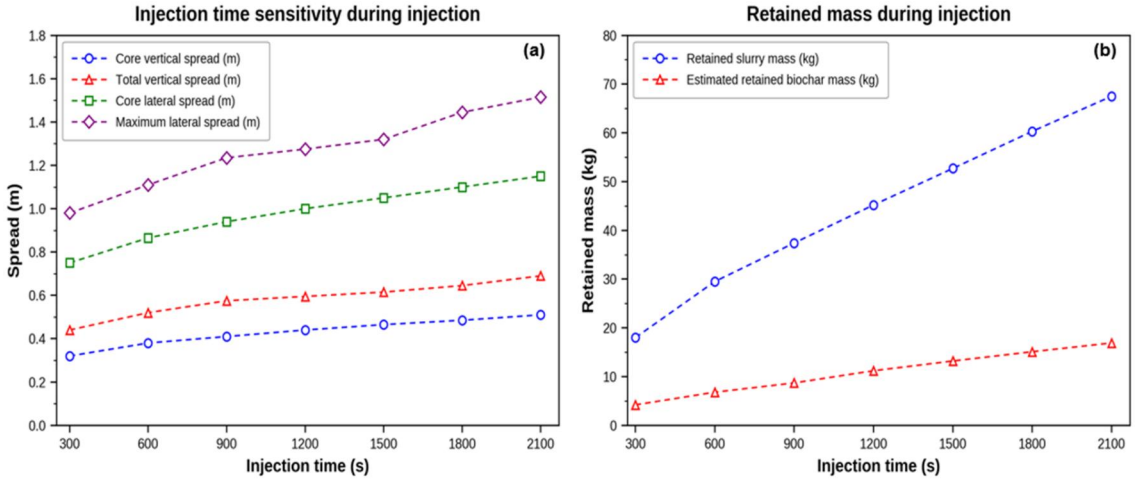

Figure 8. (a) The vertical and horizontal spreads of biochar slurry with increasing injection time and (b) the retained mass of slurry and biochar inside the soil medium at varying injection rates.

Stage of model validation

The second-stage validation was carried out by comparing the simulated saturated hydraulic conductivity (K_{sat}) of biochar-amended sand with the experimental results reported by Trifunovic et al. (2018) for the unsieved and fine biochar cases. Overall, the numerical model reproduced both datasets closely, with reported overall discrepancies of approximately 2% for the unsieved biochar case and 1% for the fine biochar case as seen in Figure 7.

For the unsieved biochar case, the simulations reproduced the non-monotonic trend observed in the experimental data. At 0% biochar content, both the experimental and numerical results gave a K_{sat} of approximately 3.0×10^{-3} m/s. As the biochar content increased to 5%, K_{sat} increased to about $3.6–3.7 \times 10^{-3}$ m/s, after which it decreased at 10% and 20% biochar content to approximately $2.8–2.9 \times 10^{-3}$ m/s and $1.5–1.6 \times 10^{-3}$ m/s, respectively. The numerical results followed the same response pattern and remained very close to the experimental values across all biochar contents. Defining porous media properties based on the Darcy conversion of K_{sat} into absolute permeability shows that the initial increase in porosity at lower clogging rates can also be simulated through the assumptions used for this model.

For the fine biochar case, both the experimental and numerical results showed a consistent monotonic decrease in K_{sat} with increasing biochar content. Starting from approximately 3.0×10^{-3} m/s at 0% biochar, the hydraulic conductivity decreased to about $2.4–2.5 \times 10^{-3}$ m/s at 5%, $1.7–1.8 \times 10^{-3}$ m/s at 10%, and $0.5–0.6 \times 10^{-3}$ m/s at 20% biochar content. The numerical simulations reproduced this decreasing trend closely, with only minor overprediction relative to the experimental measurements at the amended cases. Overall, the second-stage validation shows that the adopted porous media model was able to capture both the threshold-type response of the unsieved biochar case and the progressive reduction in hydraulic conductivity observed for the fine biochar case. This close agreement supports the suitability of the selected model parameters and numerical procedure for representing the hydraulic response of biochar-amended sand.

Numerical simulation

Injection and settling time analysis

The effect of injection time on slurry permeation was evaluated by varying the injection duration from 300 to 2100s under the baseline case of 25 kPa injection pressure, 25 BC % biochar content, and 0.3 m inlet diameter. As shown in Figure 8a, increasing the injection time increased all measured spread parameters. Core vertical spread increased from 0.314 m at 300 s to 0.505 m at 2100s, while total vertical spread increased from 0.431 to 0.676 m over the same range. Similarly, core lateral spread increased from 0.745 to 1.148 m, and maximum lateral spread increased from 0.985 to 1.519 m. The retained slurry mass also increased continuously with injection time, rising from 17.6 kg at 300 s to 67.6 kg at 2100s as seen in Figure 8b. Since the slurry loading was fixed at 25 BC %, the estimated retained

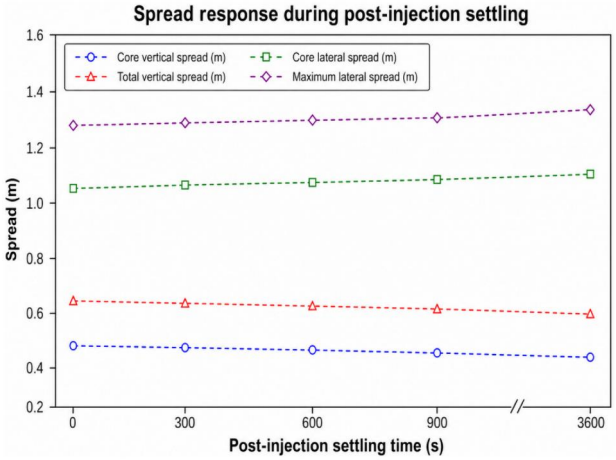

Figure 9. Post injection vertical and horizontal spread of the slurry plume with 0 kPa pressure varying with time.

biochar mass increased proportionally from 4.4 to 16.9 kg. These results indicate that longer injection duration promoted continued slurry migration and retention within the soil domain. The spread curves further show that the increase in plume extent was more pronounced during the earlier injection stages, whereas the rate of increase became smaller at later times. In particular, the interval-to-interval gains in total vertical spread and maximum lateral spread were reduced by about 1200 to 1500s, although additional growth was still observed at 1800s and 2100s. In addition, the gap between the core spread and total spread measures became larger with increasing injection time, indicating that the affected zone continued to expand beyond the main concentrated plume at later stages.

A post-injection settling analysis was also carried out by closing the inlet after 1500s of injection and monitoring the subsequent spread evolution for up to 3600s. The results as seen in Figure 9 show that the vertical spread changed only slightly during the settling period. Core vertical spread decreased from 0.463 m at inlet shutoff to 0.428 m after 1 h, while total vertical spread decreased from 0.608 to 0.592 m. In contrast, the lateral spread continued to increase after injection stopped. Core lateral spread increased from 1.051 to 1.140 m, and maximum lateral spread increased from 1.320 to 1.541 m during the same settling period. These results show that post-injection behaviour was associated mainly with lateral redistribution of the slurry plume, while further downward penetration was limited after inlet closure.

Effect of operating parameters on slurry spread and retained mass

The effects of injection pressure, inlet diameter, and biochar loading were evaluated to determine how the main operating parameters influenced slurry spread and retained mass under the field-scale conditions. As shown in Figures 10a and b, increasing injection pressure from 10 to 200 kPa increased both the plume's spread and retained mass. Core vertical spread increased from 0.352 to 0.570 m, while total vertical spread increased from 0.472 to 0.724 m. Similarly, core lateral spread increased from 0.811 to 1.222 m, and maximum lateral spread increased from 1.043 to 1.583 m. The retained slurry mass increased from 23.3 to 89.0 kg, while the retained biochar mass increased from 5.825 to 22.25 kg. This shows that higher pressure promoted both greater permeation extent and higher slurry retention within the soil domain.

A similar increasing trend was observed for inlet diameter. As shown in Figures 10c and d, increasing the inlet diameter from 0.1 to 0.5 m increased all spread and mass parameters. Core vertical spread increased from 0.254 to 0.433 m, while total vertical spread increased from 0.340 to 0.626 m. Core horizontal spread increased from 0.549 to 1.089 m, and maximum lateral spread increased from 0.710 to 1.444 m. Retained slurry mass also increased from 8.0 to 55.2 kg, while retained biochar mass increased from 2.0 to 13.8 kg. These results indicate that larger inlet diameters increased both the treatment-zone size and the amount of biochar retained during injection.

In contrast, increasing biochar loading reduced slurry spread and retained mass. As shown in Figures 10(e) and 10(f), increasing biochar content from 25 to 40 BC % decreased core vertical spread from 0.377 to 0.205 m and total vertical spread from 0.513 to 0.304 m. Core lateral spread decreased from

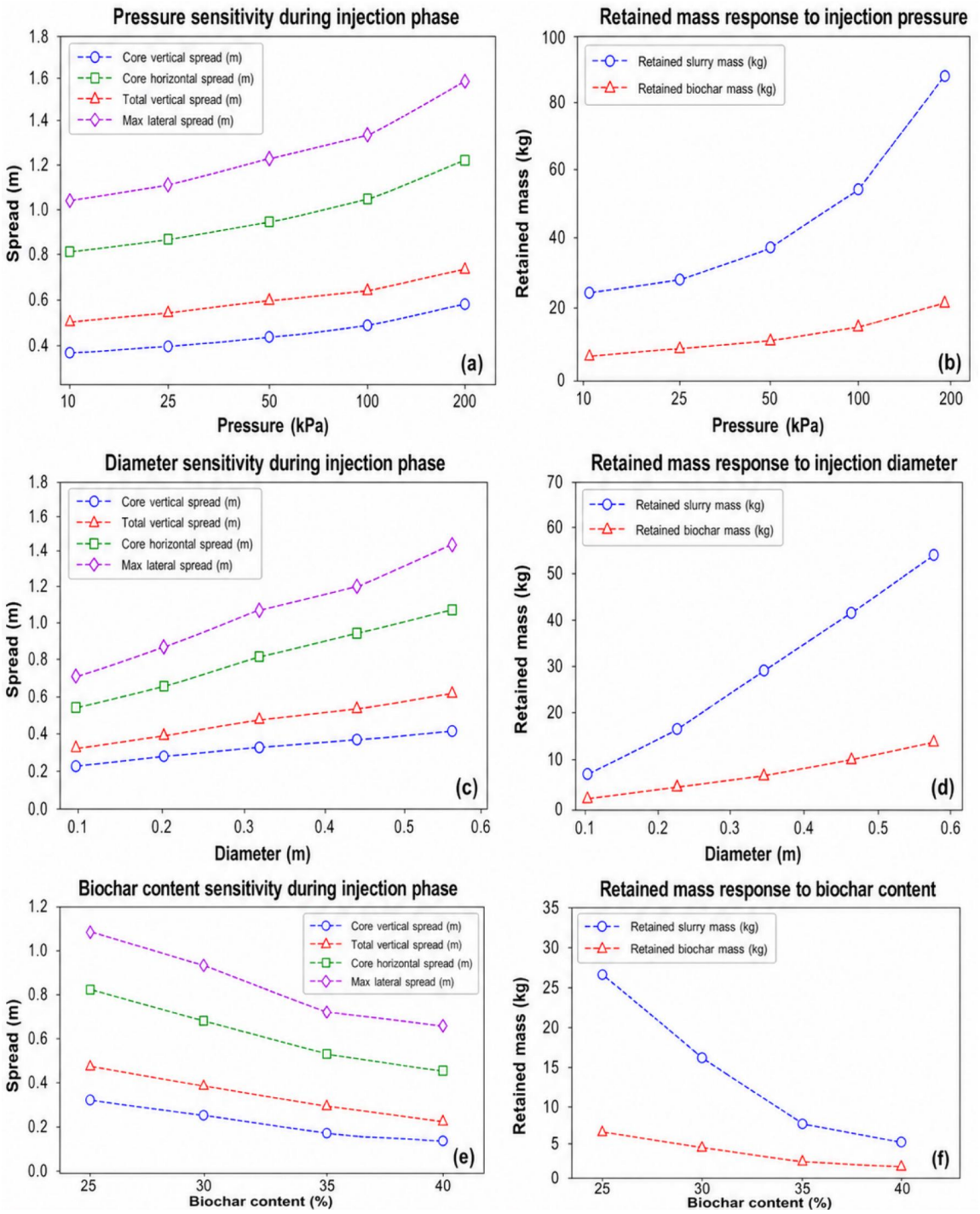

Figure 10. (a) (c) (e) Shows the vertical and horizontal spreads of slurry inside the soil medium based on pressure, diameter and BC% and (b) (d) (f) shows the retained slurry and biochar masses in the soil medium based on the same operating conditions.

0.864 to 0.549 m, while maximum lateral spread decreased from 1.112 to 0.735 m. Retained slurry mass also decreased from 28.7 to 5.25 kg, and retained biochar mass decreased from 7.175 to 2.1 kg. Therefore, unlike pressure and inlet diameter, higher biochar loading limited plume development under the same injection conditions. Overall, the combined operating-parameter results show that injection pressure and inlet diameter acted as plume-amplifying parameters, increasing both spread and retained mass. In contrast, biochar loading acted as a mobility-limiting parameter, reducing the extent of slurry migration and the amount of retained biochar as the solid content increased.

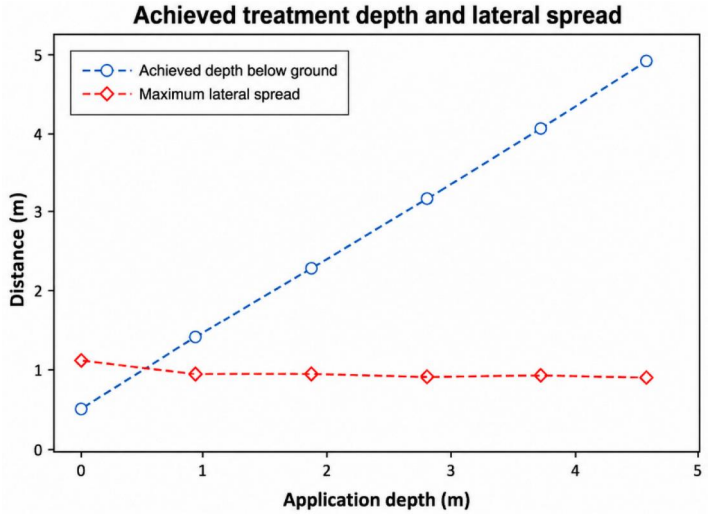

Figure 11. Variation of achieved treatment depth and maximum lateral spread with application depth for the field-scale permeation model.

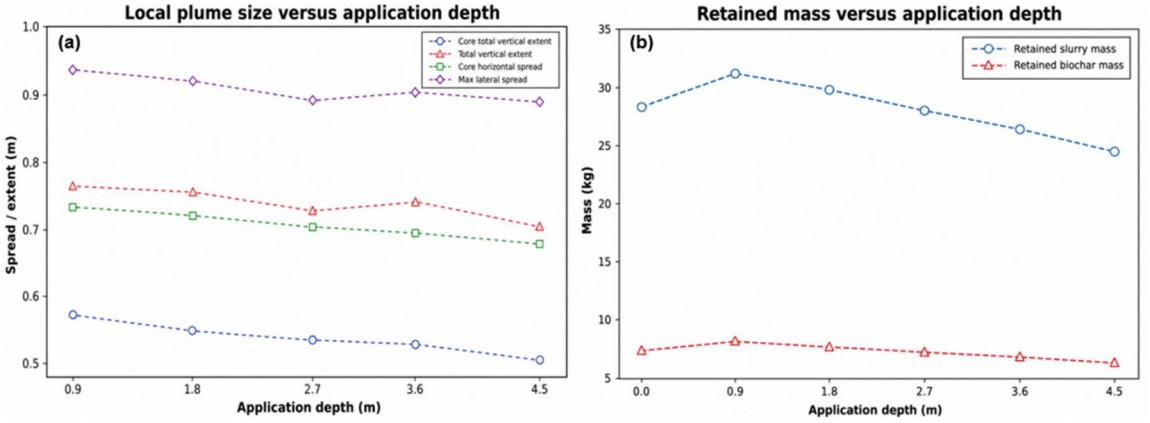

Figure 12. (a) The vertical and horizontal spreads of biochar slurry with varying application depth and (b) the retained mass of slurry and biochar inside the soil medium at varying application depths.

Depth application analysis

The effect of application depth on slurry permeation was evaluated by comparing surface injection with buried injection at depths of 0.9, 1.8, 2.7, 3.6, and 4.5 m under a constant injection pressure of 25 kPa, biochar loading of 25 BC%, inlet diameter of 0.3 m, and injection duration of 600 s. As shown in Figure 11, increasing the application depth substantially increased the achieved treatment depth below ground. For the surface case, the total vertical spread below the ground surface was 0.513 m. In contrast, the buried cases produced achieved total depths of 1.384, 2.286, 3.171, 4.080, and 4.963 m for application depths of 0.9, 1.8, 2.7, 3.6, and 4.5 m, respectively. However, the maximum lateral spread did not increase with application depth, decreasing from 1.112 m for surface injection to 0.935 m at 0.9 m depth and remaining within a narrow range of 0.890–0.917 m for the deeper buried cases. This indicates that deeper application mainly shifted the treatment zone downward rather than enlarging the local plume footprint around the injection point.

The local plume-size results as seen in Figure 12a confirm this trend. Total downward spread below the tip remained nearly constant across the buried cases, varying only from 0.484 m at 0.9 m depth to 0.463 m at 4.5 m depth. Similarly, total upward spread decreased slightly from 0.276 to 0.241 m over the same range. As a result, total vertical extent around the tip decreased only slightly from 0.760 m at 0.9 m insertion to 0.704 m at 4.5 m insertion. The same pattern was observed for the core plume, where core total vertical extent decreased from 0.567 to 0.497 m. Horizontal plume size also showed only modest variation, with core horizontal spread decreasing from 0.733 to 0.682 m and

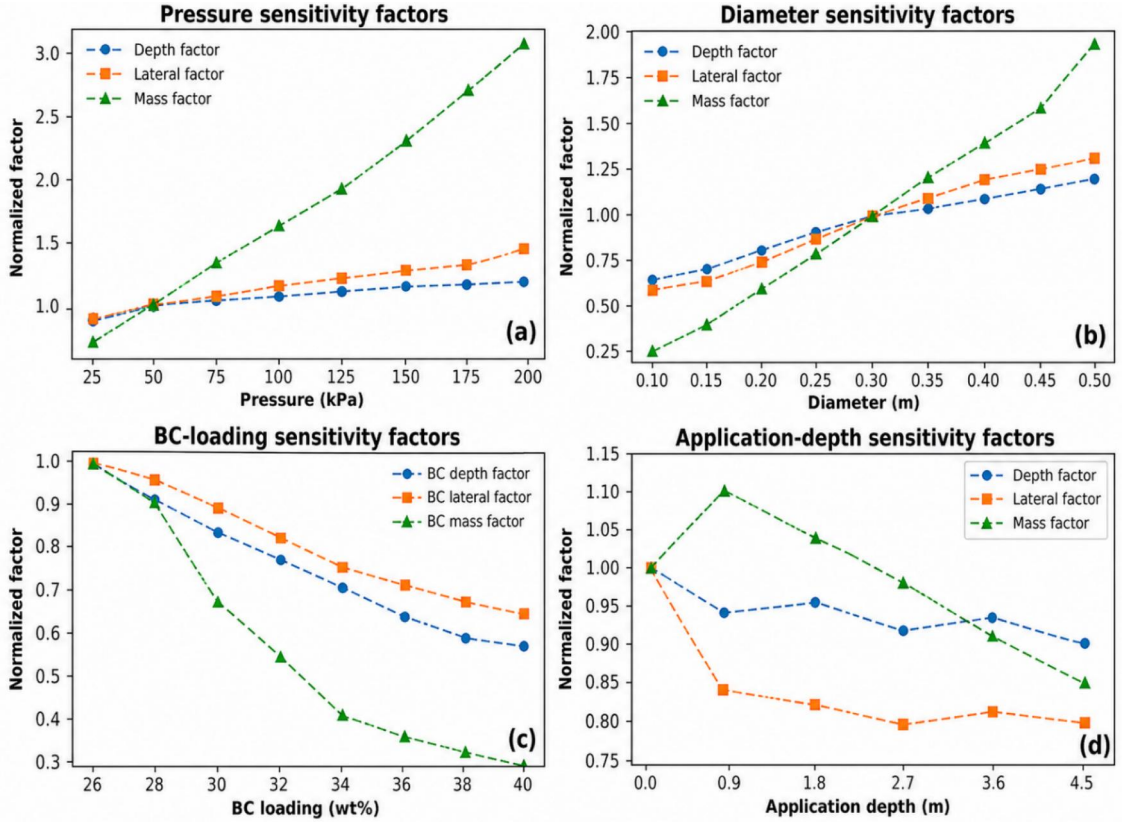

Figure 13. Normalized sensitivity factors used in the target-depth screening framework: (a) pressure factors, (b) inlet-diameter factors, (c) BC-loading factors, and (d) application-depth factors.

maximum lateral spread decreasing from 0.935 to 0.890 m as the application depth increased from 0.9 to 4.5 m. These results show that deeper insertion did not substantially enlarge the local plume around the tip.

The retained mass results observed from Figure 12b indicate that shallow buried injection provided the greatest retention. Retained slurry mass increased from 28.7 kg for the surface case to 31.6 kg at 0.9 m depth, but then decreased progressively to 29.8, 28.1, 26.4, and 24.5 kg for depths of 1.8, 2.7, 3.6, and 4.5 m, respectively. The same trend was observed for retained biochar mass, which increased from 7.175 kg for the surface case to 7.9 kg at 0.9 m depth, before decreasing to 6.125 kg at 4.5 m depth. Overall, the results show that application depth mainly influenced the final position of the treatment zone rather than the plume size itself. The shallow buried case of 0.9 m produced the highest retained slurry and biochar masses, whereas deeper application was more effective when the objective was to reach a deeper subsurface target zone.

Target depth and effective permeation

A final target-depth assessment was carried out to identify practical operating conditions capable of reaching selected subsurface treatment depths. This analysis was conducted at a fixed injection duration of 600 s using the completed sensitivity analyses for injection pressure, inlet diameter, BC%, and application depth. The reference case used for the screening framework was 25 kPa injection pressure, 0.3 m inlet diameter, 25 BC%, surface application, and 600 s injection duration. The corresponding reference values were 0.513 m for downward spread, 1.112 m for maximum lateral spread, and 7.175 kg for retained biochar mass. These values were then adjusted using normalized sensitivity factors obtained from the individual parametric studies. As shown in Figure 13a, increasing injection pressure increased the downward-spread, lateral-spread, and retained-mass factors, with the strongest increase observed for retained biochar mass. At 200 kPa, the pressure factor increased to 1.411 for downward spread, 1.424 for maximum lateral spread, and 3.101 for retained biochar mass. A similar response was observed for inlet diameter, as shown in Figure 13b. Increasing the diameter from 0.1 to 0.5 m

Table 2. Balanced and high-power candidate cases for the 3.0 and 4.0 m target-depth conditions. The operating condition column lists injection pressure, inlet diameter, BC%, and application depth, respectively.

Target depth (m)	Case type	Operating condition	Achieved depth (m)	Max lateral spread (m)	Retained biochar mass (kg)
3.0	Balanced Design	25 kPa, 0.3 m, 25 BC%, 2.7 m Depth	3.171	0.893	7.025
3.0	High power design	200 kPa, 0.5 m, 25 BC%, 2.7 m Depth	3.511	1.652	41.896
4.0	Balanced Design	25 kPa, 0.3 m, 25 BC%, 3.6 m Depth	4.080	0.909	6.600
4.0	High power design	200 kPa, 0.5 m, 25 BC%, 3.6 m Depth	4.427	1.681	39.371

increased the downward-spread factor from 0.663 to 1.220, the lateral-spread factor from 0.639 to 1.299, and the retained-mass factor from 0.279 to 1.923. Therefore, both injection pressure and inlet diameter acted as plume-amplifying parameters in the screening framework. In contrast, the BC-loading factors showed a decreasing trend with increasing BC%, as shown in Figure 13c. Increasing BC% from 25 to 40 reduced the downward-spread factor from 1.000 to 0.593, the lateral-spread factor from 1.000 to 0.661, and the retained-mass factor from 1.000 to 0.293. This indicates that increasing BC% reduced slurry mobility and retained biochar mass under the tested pressure-driven conditions. Accordingly, 25 BC% was retained as the preferred loading for the final target-depth assessment. The application-depth factors shown in Figure 13d further indicate that local downward spread remained relatively stable with increasing insertion depth, while lateral spread and retained biochar mass generally decreased. This confirms that application depth primarily acted as a positioning parameter, whereas pressure and inlet diameter mainly controlled plume amplification and mass delivery.

Based on the buried-injection results, the downward spread below the injection tip remained relatively stable across the tested insertion depths, ranging from 0.463 to 0.486 m. The mean downward spread was approximately 0.477 m and was rounded to 0.48 m for preliminary target-depth estimation. Therefore, the required insertion depth was first estimated using $d_{a,req} \approx z_t - 0.48$, where z_t is the target treatment depth. This relation was used only as an initial estimate, while the final cases were assessed using the full factor-based screening procedure. Two target depths were selected for final comparison: 3.0 m as the primary target depth and 4.0 m as the higher-demand target depth. For the 3.0 m target, the balanced design case corresponded to 25 kPa injection pressure, 0.3 m inlet diameter, 25 BC%, and 2.7 m application depth. As shown in Table 2, this case achieved a final treatment depth of 3.171 m, with a maximum lateral spread of 0.893 m and retained biochar mass of 7.025 kg. The corresponding high-power envelope case, using 200 kPa and 0.5 m diameter at the same application depth, was predicted to reach 3.511 m and retain 41.896 kg of biochar, but with a substantially larger lateral spread of 1.652 m. Therefore, the balanced case was sufficient to meet the 3.0 m target while maintaining a more controlled treatment footprint. For the 4.0 m target, the balanced design case was obtained using 25 kPa injection pressure, 0.3 m inlet diameter, 25 BC%, and 3.6 m application depth. This case achieved a final treatment depth of 4.080 m, with a maximum lateral spread of 0.909 m and retained biochar mass of 6.600 kg. The corresponding high-power envelope case reached 4.427 m and retained 39.371 kg of biochar, but the maximum lateral spread increased to 1.681 m. This again shows that increasing pressure and inlet diameter can increase plume size and retained mass, but at the cost of a wider treatment footprint. Therefore, the high-power cases are more suitable as upper-bound envelope scenarios, whereas the moderate-pressure and moderate-diameter cases represent the preferred practical design conditions. Overall, the target-depth assessment shows that the required treatment depth can be achieved most effectively by adjusting the application depth. Pressure and inlet diameter should instead be treated as parameters for tuning the local plume size and retained mass. Therefore, the final design logic is to use insertion depth to place the biochar plume at the required subsurface target, maintain 25 BC% to preserve slurry mobility, and increase pressure or inlet diameter only when a larger treatment footprint or higher retained mass is required.

Discussion

Reliability of the numerical framework

The two-stage validation strategy was important for establishing the reliability of the numerical framework before extending the analysis to field-scale biochar slurry permeation. The first stage served primarily as a hydraulic verification step, confirming that the assigned porous-medium properties and pressure-based boundary conditions produced a physically consistent steady-state pressure-loss response through the saturated soil domain similar to such numerical simulations in various literature (Alam et al. 2020; Diana et al. 2021). This step was necessary because the subsequent slurry simulations rely on the correct implementation of the porous-media resistance formulation in ANSYS Fluent, where pressure loss through a porous region is represented using momentum source terms associated with viscous and, when required, inertial resistance (ANSYS 2009). However, this stage should not be interpreted as a direct experimental validation, since its purpose was to confirm the hydraulic behaviour of the base porous medium rather than reproduce an external dataset.

The second validation stage provided the main experimental comparison by evaluating the model response against the biochar-amended sand data reported by Trifunovic et al. (2018). This dataset was suitable for validation because it used a well-defined homogeneous Ottawa sand medium and examined the effects of biochar concentration and particle-size distribution on saturated hydraulic conductivity. The model reproduced both the non-monotonic K_{sat} response observed for the unsieved biochar case and the monotonic reduction in K_{sat} observed for the fine biochar case. This is important because *Trifunovic et al.* (2018) showed that the hydraulic behaviour of biochar-amended sand depends not only on biochar concentration, but also on the relative proportion of fine biochar particles capable of occupying pore spaces and modifying the pore structure. Therefore, agreement with both particle-size cases indicates that the adopted numerical framework was able to represent the bulk hydraulic effect of biochar amendment on sandy soil. At the same time, the validation should be interpreted at the continuum hydraulic-response level. The agreement with literature K_{sat} data demonstrates that the bulk permeability behavior of biochar-amended sand can be represented with satisfactory accuracy, but it does not imply that pore-scale particle interactions, transient clogging development, or particle-size-specific deposition were directly resolved. These mechanisms were treated implicitly through the effective hydraulic properties and model assumptions. Accordingly, the validated framework provides a suitable basis for assessing average slurry permeation behavior, while more detailed particle-scale mechanisms remain a subject for future model development.

Time sensitivity of permeation and post-injection redistribution

The injection-time analysis shows that biochar slurry permeation is strongly time-dependent under continued pressure-driven injection. Increasing injection duration increased the vertical and lateral spread of the plume, as well as the retained slurry and retained biochar mass. This response is expected because longer injection allows the pressure gradient to act over a longer period, increasing the cumulative volume of slurry entering the porous domain. Similar behaviour has been reported in permeation grouting studies, where injection time, flow rate, and pressure are directly related to the development of grout diffusion radius and treated-zone size (Celik 2019; Zhou et al. 2021; Hu et al. 2024). However, the results also showed that the increase in plume extent became less pronounced after approximately 1200–1500s. This suggests that the practical benefit of continued injection decreases with time, even though the plume did not reach a complete plateau within the tested range. In the present model, this trend should be interpreted as a reduction in incremental spread gain under continued constant-pressure injection rather than as direct evidence of clogging. Since the porous resistance and porosity were kept fixed during the time-sensitivity analysis, the model does not explicitly simulate time-dependent pore blocking, filtration, or permeability reduction. Therefore, the observed diminishing gain is more appropriately described as progressive plume expansion with reduced marginal increase at later injection times.

The post-injection settling results further show that once the inlet was closed, additional downward movement was limited. Vertical spread decreased slightly after shutoff, while lateral spread continued

to increase. This indicates that the post-injection stage was dominated by redistribution of the slurry plume within the already affected region rather than continued penetration to greater depth. Similar time-dependent redistribution behaviour is relevant in slurry and grouting problems, where the final treatment geometry is controlled not only by the active injection stage but also by the subsequent relaxation and redistribution of the injected material after pressure release (Li et al. 2022; Hu et al. 2024).

Although extending injection time increased slurry delivery and retained biochar mass, this response should be interpreted as an upper-bound estimate because transient clogging and permeability evolution were not included. In real particulate slurry permeation, retained particles can progressively block pore throats, form filtration zones or filter cakes, and reduce permeability, thereby limiting later-stage penetration. Similar behaviour has been reported in cement-grouting studies, where filtration reduces permeability and causes penetration rate or diffusion radius to decrease or stabilize with time (Sun et al. 2019; Yang et al. 2025). Therefore, incorporating transient clogging would likely reduce the predicted spread at longer injection durations.

Governing controls on biochar slurry permeation

The field-scale sensitivity results indicate that biochar slurry permeation is governed by a combination of hydraulic driving conditions, inlet geometry, slurry composition, and application depth. However, these parameters did not influence the permeation response in the same manner. Injection pressure and inlet diameter generally acted as plume-amplifying parameters, as both increased the vertical spread, lateral spread, retained slurry mass, and retained biochar mass. This behaviour is consistent with permeation grouting and slurry-injection studies, where higher grouting pressure and injection geometry have been shown to increase the diffusion radius, penetration extent, and treated-zone size in porous or saturated sandy media (Celik 2019; Zhou et al. 2021; Li et al. 2022; Hu et al. 2024). Higher injection pressure increases the pressure gradient available to drive slurry through the saturated pore network, while a larger inlet diameter increases the effective injection footprint and allows a greater volume of slurry to enter the soil over the same injection period. Similar relationships between injection pressure, penetration distance, and grout diffusion have been reported in numerical and experimental grouting studies, where increased pressure generally promotes larger propagation zones but may also increase the lateral extent of the treated region (Zhou et al. 2021; Li et al. 2022). While pressure and diameter improved slurry delivery in the present model, they also enlarged the treatment footprint.

In comparison, increasing BC% reduced slurry mobility. This trend is consistent with the rheological behaviour of biochar-water slurry reported by Liu et al. (2017) which showed that slurry viscosity and stability are strongly affected by biochar solid content, particle size, and particle-size distribution. As BC% increases, the effective viscosity of the slurry also increases, which restricts its ability to permeate the porous soil within the same injection duration. Therefore, while a higher BC% may appear beneficial from a carbon-loading perspective, the present results suggest that excessive solid loading can reduce the actual amount of biochar delivered and retained in the soil under pressure-controlled injection. However, increasing the injection pressure and diameter could allow for higher spread and retained slurry mass in soil although it may result in exceeding the threshold for permeation grouting pressure resulting in fractures (Liu et al. 2023). The observed reduction in mobility at higher BC% also agrees with broader biochar–soil hydraulic studies showing that biochar particle size, concentration, pore occupation, and pore-size redistribution can strongly affect water movement in amended soils (Githinji 2014; Jun Zhang et al. 2016; Trifunovic et al. 2018; Chen et al. 2022; Jia et al. 2024). In particular, Trifunovic et al. (2018) showed that fine biochar particles can reduce saturated hydraulic conductivity by occupying pore spaces and increasing tortuosity in sand. However, in the present CFD model, this effect should be interpreted carefully as the reduction in spread with increasing BC% is mainly represented through the effective viscosity and bulk slurry properties, rather than through explicitly resolved particle bridging or time-dependent pore clogging.

Application depth and target zone delivery

The application-depth analysis showed that insertion depth played a different role from pressure, inlet diameter, and BC%. While pressure and inlet diameter mainly changed the size of the plume, application depth primarily controlled the final position of the treatment zone below ground. This is important because the main purpose of the proposed permeation approach is not only to increase local slurry spread, but to place biochar at a required subsurface depth. In this regard, the results suggest that deeper application is most useful as a positioning mechanism, rather than as a direct method for increasing plume size around the injection point. The local plume-size results support this interpretation. Although the achieved treatment depth increased substantially with increasing application depth, the downward spread below the injection tip remained nearly constant with a slight decrease. The slight reduction in local plume size at greater application depths may be explained by the more confined buried-injection condition and increased resistance to redistribution around the outlet (Ding et al. 2024). Grouting studies have reported that, under the same grouting pressure, injectable grout volume can decrease with increasing burial depth as confining pressure becomes more influential, and that permeation is controlled by the interaction between slurry properties and the pore structure of the surrounding medium (Xu et al. 2023). As this study was a pressure-driven simulation, the local slight decrease aligns with these findings. It should also be noted that the plume spread may decrease at deeper depths due to overburden pressure on the soil restricting pores and thereby reducing permeability (Wang et al. 2023). Therefore, deeper application mainly repositioned the plume rather than increasing local expansion around the injection point. This indicates that the deeper cases reached greater total depths mainly because the injection point itself was placed deeper, not because the slurry travelled much farther below the tip. Therefore, the application depth can be interpreted as a geometric control on target-zone placement. This behaviour is also consistent with permeation-based injection principles, where the final treated region is governed by both the location of the injection source and the local diffusion of the injected material around that source (Celik 2019; Zhou et al. 2021; Li et al. 2022).

The retained-mass trend further shows that deeper insertion is not always better from a delivery-efficiency perspective. The shallow buried case produced the highest retained slurry and retained biochar mass, while further increases in application depth gradually reduced retention. This suggests that shallow subsurface placement may provide improved confinement compared with surface injection, but deeper insertion can introduce a trade-off where the target depth is reached at the expense of lower retained mass and slightly smaller local plume size which is consistent with the findings of Ding et al. (2024). Therefore, the preferred application depth depends on the design objective. If the objective is maximum retained mass, a shallower buried depth is more favourable. If the objective is to reach a deeper target zone, deeper insertion becomes necessary even if retention decreases slightly.

This finding is particularly relevant to the practice deficiency identified in the introduction. Conventional biochar application is commonly associated with surface or shallow incorporation, which may be suitable for agricultural amendment but is less effective when the objective is controlled deep placement. Previous biochar application guidance and reviews have also highlighted practical challenges associated with field application, including handling, mixing, erosion risk, and the need for appropriate placement methods (Major 2010; Verheijen et al. 2010; El-Naggar et al. 2019; Campion et al. 2023). The present results address this gap by showing that application depth can be used to position the biochar treatment zone more deliberately within the subsurface, without relying only on increasing pressure or inlet diameter.

The target-depth analysis strengthens this interpretation. For both the 3.0 and 4.0 m target depths, the balanced cases achieved the required treatment depth using moderate pressure, moderate inlet diameter, and 25 BC%, provided that the injection point was placed at the appropriate application depth. In contrast, the high-power cases increased retained biochar mass and plume size, but also produced a much wider lateral footprint. This means that pressure and diameter are useful for enlarging the treated zone, but they are not the most efficient way to control depth achievement. The more practical design logic is to first select the application depth based on the target zone, and then adjust pressure and inlet diameter only to tune the local plume size and retained mass.

Practical design implications

The results of this study provide a practical basis for selecting field-scale biochar slurry permeation conditions according to the intended treatment objective. The target-depth analysis showed that the required subsurface depth can be achieved most effectively by selecting an appropriate application depth, while injection pressure and inlet diameter should be used mainly to adjust the local plume size and retained biochar mass. This distinction is important because increasing pressure or diameter from the surface may enlarge the treated zone, but it does not provide the same level of control over where the biochar is placed vertically. Therefore, for deep biochar insertion, application depth should be treated as the primary design variable, while pressure and diameter should be treated as secondary tuning parameters.

From a practical design perspective, the balanced cases were more favourable than the high-power cases. For both the 3.0 and 4.0 m target depths, moderate conditions using 25 kPa injection pressure, 0.3 m inlet diameter, and 25 BC% were sufficient to reach the required treatment depth when the application depth was selected appropriately. In contrast, the high-power cases using 200 kPa and 0.5 m diameter increased the retained biochar mass, but also produced a much wider lateral spread. This indicates that maximum pressure and maximum inlet diameter are not necessarily the most efficient options if the objective is controlled deep placement. Instead, these higher-intensity cases are better interpreted as upper-bound scenarios for cases where a larger treatment footprint or greater mass delivery is acceptable. The higher-intensity cases also present a higher chance for fracture occurrence, which disturbs the soil stratum (Liu et al. 2023) and could result in soil strength losses (Wang et al. 2026). Such losses could lead to preferential leaching resulting in biochar particles moving into groundwater rather than being sequestered in the soil matrix itself (Zuolin Liu et al. 2016).

The results also show that higher BC% should not automatically be selected for carbon sequestration purposes. Although increasing BC% increases the amount of biochar per unit mass of slurry, the simulations showed that higher BC% reduced slurry mobility, plume spread, and retained biochar mass under the same pressure-driven conditions. Therefore, the most suitable slurry loading is not simply the highest available BC%, but the concentration that maintains sufficient mobility for soil permeation while still delivering a meaningful amount of biochar. In the present framework, 25 BC% provided the best balance between mobility and retained biochar mass. While potential for higher BC% sequestration exists, effective permeation can only be achieved through higher inlet diameter and pressures and injection times which risks the occurrence of fractures in soil.

These findings are relevant to the practical deficiency of conventional biochar application methods. Surface spreading and mechanical mixing can be appropriate for shallow soil amendment, but they are less suitable when the objective is controlled deep insertion. Previous reviews and practical guidelines have noted that biochar field application can be limited by handling, labour, cost, erosion risk, and the difficulty of achieving uniform placement, particularly when large-scale application is considered (Major 2010; Verheijen et al. 2010; El-Naggar et al. 2019; Campion et al. 2023). The present results suggest that pressure-driven slurry permeation could provide a more targeted route for subsurface delivery, as the application depth can be selected to place the treatment zone at the desired depth without relying solely on extensive surface mixing.

Model limitations and future improvements

The present study provides a continuum-scale assessment of biochar slurry permeation through saturated sandy soil; however, several model limitations should be acknowledged. First, the soil domain was assumed to be homogeneous, isotropic, rigid, and fully saturated. This assumption allowed the effect of pressure-driven slurry permeation to be isolated, but it does not account for natural field variability such as stratification, preferential flow paths, partial saturation, or spatial changes in permeability. Since field soils are rarely uniform, the predicted plume geometry should be interpreted as an idealized response under controlled porous-medium conditions rather than a direct representation of all possible field conditions.

Second, the biochar slurry was represented using effective bulk properties, including literature-derived apparent viscosity values. This approach was necessary because limited experimental data are available on biochar-water slurry rheology, and Liu et al. (2017) remains one of the few studies reporting viscosity behaviour for biochar slurry over different solid contents and particle-size conditions. However, biochar slurry is a particulate suspension and cannot be treated as equivalent to water. Its behaviour depends on solid content, particle size, particle-size distribution, water uptake, and shear-dependent rheology (Liu et al. 2017). Therefore, the present model captures the average flow behaviour of the slurry, but does not fully resolve non-Newtonian effects, particle segregation, aggregation, or local changes in concentration during permeation.

Another important limitation is that transient clogging and permeability evolution were not explicitly included. The porous resistance and porosity were kept fixed during the field-scale simulations, meaning that particle deposition, pore-throat blocking, filtration effects, and time-dependent reductions in hydraulic conductivity were not directly simulated. This is particularly relevant because biochar-amended sand studies have shown that fine biochar particles can occupy pore spaces, alter pore-size distribution, increase tortuosity, and reduce saturated hydraulic conductivity (Trifunovic et al. 2018; Chen et al. 2022). As a result, the predicted spread at longer injection times may represent an upper-bound estimate under constant-pressure conditions. If progressive clogging and permeability reduction were included, the later-stage plume growth would likely be more restricted. The model also did not explicitly resolve the internal pore structure of individual biochar particles. Biochar contains open and closed intra-particle pores (Yong Wan et al. 2022), which may influence water uptake, apparent particle density, slurry viscosity, and interaction with soil pores. In the present formulation, these structural effects were embedded indirectly through effective slurry properties rather than being modelled at the particle scale. This simplification is acceptable for continuum-scale permeation analysis, but it limits the ability of the model to describe detailed biochar-water-soil interactions at the pore or particle level.

Future work should therefore focus on improving the physical representation of biochar transport and retention in soil. A more advanced model could include transient clogging relationships, permeability reduction functions, or evolving porosity linked to local biochar retention. Particle-resolved approaches, such as CFD–DEM coupling, would also be useful for studying interparticle interactions between biochar and sand, particle bridging, pore blocking, and deposition mechanisms. Similar coupled approaches have been used in grouting studies to represent particle-scale slurry movement in saturated granular media (Li et al. 2022). In addition, future simulations should consider heterogeneous soils, partial saturation, different biochar particle-size distributions, and experimentally measured slurry rheology for the specific biochar source used. Finally, further experimental validation is necessary before the proposed permeation approach can be considered field-ready. Laboratory column tests and pilot-scale injection studies would allow the predicted spread, retained biochar mass, and target-depth delivery to be compared directly with measured data. Such validation would also help determine whether the simulated treatment zones remain stable over time, especially under realistic drainage, wetting-drying, freeze-thaw, and soil-structure conditions. Therefore, while the present model provides a useful first step in evaluating pressure-driven biochar slurry permeation, future studies should extend the framework toward transient clogging, particle-scale transport, and experimental field-scale verification.

Conclusions

This study evaluated the feasibility of pressure-driven biochar slurry permeation as a potential method for targeted subsurface biochar insertion in sandy soil. A coupled multiphase porous-media CFD framework was developed and validated in two stages. The first stage confirmed that the porous-media setup produced a physically consistent pressure-loss response, while the second stage showed close agreement with the experimental K_{sat} trends reported for biochar-amended sand. The model was able to reproduce both the non-monotonic response of unsieved biochar and the monotonic reduction in hydraulic conductivity observed for fine biochar, supporting its suitability for representing the bulk hydraulic response of biochar-modified sandy soil.

The field-scale simulations showed that injection time, pressure, inlet diameter, BC%, and application depth influenced slurry permeation in different ways. Increasing injection time promoted plume growth and retained biochar mass, although the later-stage gains became less pronounced. Injection pressure and inlet diameter acted as plume-amplifying parameters, increasing both spread and retained mass. In contrast, increasing BC% reduced slurry mobility, resulting in smaller plume spread and lower retained biochar mass under the same pressure-driven conditions. Application depth behaved differently from the other parameters, as it primarily controlled the final position of the treatment zone rather than substantially increasing the local plume size around the injection point.

The target-depth assessment showed that the required subsurface treatment depth could be achieved more effectively by selecting an appropriate application depth rather than relying only on higher pressure or larger inlet diameter. For the 3.0 m target depth, the balanced case of 25 kPa pressure, 0.3 m inlet diameter, 25 BC%, and 2.7 m application depth achieved a final depth of 3.171 m with a controlled maximum lateral spread of 0.893 m. For the 4.0 m target depth, the corresponding balanced case at 3.6 m application depth achieved 4.080 m with a maximum lateral spread of 0.909 m. Although higher-pressure and larger-diameter cases increased retained biochar mass, they also produced wider treatment footprints, making them more suitable as upper-bound scenarios rather than preferred practical design cases.

The main contribution to knowledge is that this study advances biochar-based carbon sequestration research beyond conventional surface mixing and pre-mixed biochar-amended soil assessment by introducing a numerical framework for evaluating pressure-driven biochar slurry delivery into sandy porous media. It also contributes to permeation-method research by demonstrating how slurry rheology, injection pressure, inlet geometry, and application depth collectively influence subsurface biochar placement. In addition, the study contributes to coupled multiphase porous-media modelling by adapting a CFD-based mixture and porous-media formulation to assess the average continuum-scale behaviour of biochar slurry permeation, while clearly identifying the limits of this approach in relation to transient clogging and particle-scale deposition. The main contribution to practice is the development of a design-oriented interpretation for field-scale biochar insertion. The results suggest that application depth should be used as the primary control for reaching the target treatment zone, while injection pressure and inlet diameter should be adjusted to tune the local plume size and retained mass. BC% should be selected carefully because higher solid content does not necessarily improve delivery if slurry mobility is reduced. Therefore, for sandy soils, a balanced design approach based on insertion depth, moderate pressure, practical inlet diameter, and suitable slurry dosage may provide a more controlled pathway for deep biochar placement than conventional shallow mixing or high-power injection alone.

Overall, the study supports the potential of biochar slurry permeation as a practical route for deeper subsurface biochar delivery and carbon sequestration in sandy soils. However, future work should incorporate transient clogging, evolving permeability, particle-size-specific transport, soil heterogeneity, and experimental field or column-scale validation to further improve predictive reliability and practical applicability.

Acknowledgments

The first author acknowledges Monash University Malaysia for providing a fee waiver for his Master of Engineering Science (Research) Course.

Author contributions

CRediT: **Absam Moosa Ali**: Formal analysis, Investigation, Methodology, Software, Validation, Writing – original draft; **Mavinakere Eshwaraiah Raghunandan**: Conceptualization, Formal analysis, Investigation, Methodology, Supervision, Validation, Writing – review & editing.

Disclosure statement

The authors declare that they have no known competing financial interests or personal relationships that could have appeared to influence the work reported in this paper.

Funding

This research did not receive any specific grant from funding agencies in the public, commercial, or not-for-profit sectors.

Abbreviations

BAS	Biochar Amended Soil
CFD	Computational Fluid Dynamics
OMC	Optimal Moisture Content
FEM	Finite Element Method
VoF	Volume of Fluid
DEM	Discrete Element Method

Notations

K_{sat}	Saturated Hydraulic Conductivity
BC%	Biochar Content by %
Pg C yr^{-1}	Pentagrams of Carbon per Year
S_i	Source Term in i-directions
ν	Fluid Velocity
μ	Viscosity of relevant fluid
ρ	Density of relevant material
ρ_m	Mixture Density
ϑ_m	Mixture Velocity
κ	Intrinsic Permeability
g	Gravitational Value
n_f	Fluid Porosity
n_s	Solid Porosity
$\frac{1}{\alpha}$	Viscous Resistance
Q	Volumetric Flow Rate
A	Area of Permeation
d_{10}	10% Diameter Particle Value
d_{50}	50% Diameter Particle Value
d_{90}	90% Diameter Particle Value

References

Abdo AI. 2021. Changes in sandy soil hydro-physical properties as function of biochar and biogas slurry amendments. Soil Use Manage. 37(4):762–771. https://doi.org/10.1111/sum.12650

Alam J, Muzzammil M, Kafi M, Haque MU. 2020. An experimental and simulation study of flow through stratified soils. Water Energy Int. 63:60–72.

ANSYS I. 2009. ANSYS FLUENT 12.0/12.1 Documentation. edited.

Auger Torque. n.d. Earth drill range – mini excavators 750 kg to 3 t. in *Auger Torque Malaysia* edited.

Barbhuiya S, Bhusan Das B, Kanavaris F. 2024. Biochar-concrete: a comprehensive review of properties, production and sustainability. Case Stud Constr Mater. 20:e02859. https://doi.org/10.1016/j.cscm.2024.e02859

Bohara H et al. 2019. Influence of poultry litter and biochar on soil water dynamics and nutrient leaching from a very fine sandy loam soil. Soil Tillage Res. 189:44–51. https://doi.org/10.1016/j.still.2019.01.001

Brockhoff SR, Christians NE, Killorn RJ, Horton R, Davis DD. 2010. Physical and mineral-nutrition properties of sand-based turfgrass root zones amended with biochar. Agron J. 102(6):1627–1631. https://doi.org/10.2134/agronj2010.0188

Brown RW et al. 2023. Biochar application to temperate grasslands: challenges and opportunities for delivering multiple ecosystem services. Biochar. 5(1):33. https://doi.org/10.1007/s42773-023-00232-y

Campion L, Bekchanova M, Malina R, Kuppens T. 2023. The costs and benefits of biochar production and use: a systematic review. J Cleaner Prod. 408:137138. https://doi.org/10.1016/j.jclepro.2023.137138

Celik F. 2019. The observation of permeation grouting method as soil improvement technique with different grout flow models. Geomechanics and Engineering. 17(4):367–374. https://doi.org/10.12989/gae.2019.17.4.367

Chen Z, Kamchoom V, Apriyono A, Chen R, Chen C. 2022. Laboratory study of water infiltration and evaporation in biochar-amended landfill covers under extreme climate. Waste Manag. 153:323–334. https://doi.org/10.1016/j.wasman.2022.09.015

Chen Z, Kamchoom V, Leung AK, Xue J, Chen R. 2023. Influence of biochar on the water permeability of compacted clay subjected to freezing–thawing cycles. Acta Geophys. 72(3):2071–2081. https://doi.org/10.1007/s11600-023-01141-1

Diana B-J et al. 2021. A CFD porous materials model to test soil enriched with nanostructured zeolite using ANSYS-Fluent(TM). in Applications of computational fluid dynamics simulation and modelling, edited by B. Suvanjan, p. Ch. 5. IntechOpen. https://doi.org/10.5772/intechopen.100487
Ding B, Lou P, Huang C, Li W, Wang Y. 2024. Investigating grouting body nonuniform expansion in anisotropic underground soil mechanics. Sci Rep. 14(1):32004. https://doi.org/10.1038/s41598-024-83492-3
Edeh IG, Mašek O. 2022. The role of biochar particle size and hydrophobicity in improving soil hydraulic properties. European J Soil Science. 73(1):e13138. https://doi.org/10.1111/ejss.13138
El-Naggar A et al. 2019. Biochar application to low fertility soils: a review of current status, and future prospects. Geoderma. 337:536–554. https://doi.org/10.1016/j.geoderma.2018.09.034
Evans W, Jonson D, Walker M. 2016. An Eulerian approach to soil impact analysis for crashworthiness applications. Int J Impact Eng. 91:14–24. https://doi.org/10.1016/j.ijimpeng.2015.12.011
Genc O, Kurt A, Yazan DM, Erdis E. 2020. Circular eco-industrial park design inspired by nature: an integrated non-linear optimization, location, and food web analysis. J Environ Manage. 270:110866. https://doi.org/10.1016/j.jenvman.2020.110866
Genc O, Kurt A. 2024. Mimicking nature to design eco-industrial parks: exploring the influence of connectance on industrial network optimization. J Cleaner Prod. 475:143704. https://doi.org/10.1016/j.jclepro.2024.143704
Genc O. 2021. SymbioConstruction: a bibliography-driven dynamic construction industry symbiosis database. J Constr Eng Manage. 147(8):04021077. https://doi.org/10.1061/(ASCE)CO.1943-7862.0002095
Genc O. 2022. An assessment of transforming a city into a construction sector metabolism via industrial symbiosis implementations. Int J Civ Eng. 20(12):1495–1514. https://doi.org/10.1007/s40999-022-00765-6
Githinji L. 2014. Effect of biochar application rate on soil physical and hydraulic properties of a sandy loam. Arch Agron Soil Sci. 60(4):457–470. https://doi.org/10.1080/03650340.2013.821698
He M et al. 2021. A critical review on performance indicators for evaluating soil biota and soil health of biochar-amended soils. J Hazard Mater. 414:125378. https://doi.org/10.1016/j.jhazmat.2021.125378
Himanshu K et al. 2019. Erodibility assessment of compacted biochar amended soil for geo-environmental applications. Sci Total Environ. 672:698–707. https://doi.org/10.1016/j.scitotenv.2019.03.417
Hu H et al. 2024. Experimental study on grout–soil interaction effects in sandy soil under different water-to-cement ratios. Buildings. 14(4):947. https://doi.org/10.3390/buildings14040947
Ibitoye SE et al. 2024. An overview of biochar production techniques and application in iron and steel industries. Bioresour Bioprocess. 11(1):65. https://doi.org/10.1186/s40643-024-00779-z
James AT, James RK, Dean EA. 1999. Unsaturated zone hydrology for scientists and engineers. Prentice Hall.
Jia A et al. 2024. Biochar enhances soil hydrological function by improving the pore structure of saline soil. Agric Water Manage. 306:109170. https://doi.org/10.1016/j.agwat.2024.109170
Jien S-H, Wang C-S. 2013. Effects of biochar on soil properties and erosion potential in a highly weathered soil. CATENA. 110:225–233. https://doi.org/10.1016/j.catena.2013.06.021
Lehmann J, Gaunt J, Rondon M. 2006. Sequestration in terrestrial ecosystems – a review. Mitig Adapt Strat Glob Change. 11(2):403–427. https://doi.org/10.1007/s11027-005-9006-5
Li H, Ji X, Zhou P. 2022. Study on the microscopic mechanism of grouting in saturated water-bearing sand stratum based on VOF-DEM method. Processes. 10(8):1447. https://doi.org/10.3390/pr10081447
Liu G et al. 2023. Permeation grouting of low-permeability silty sands with colloidal silica. Case Stud Constr Mater. 19:e02327. https://doi.org/10.1016/j.cscm.2023.e02327
Liu P et al. 2017. Rheological behaviour and stability characteristics of biochar-water slurry fuels: effect of biochar particle size and size distribution. Fuel Process Technol. 156:27–32. https://doi.org/10.1016/j.fuproc.2016.09.030
Liu Z et al. 2016. Impacts of biochar concentration and particle size on hydraulic conductivity and DOC leaching of biochar–sand mixtures. J Hydrol. 533:461–472. https://doi.org/10.1016/j.jhydrol.2015.12.007
Liu Z, Ogunmokun FA, Wallach R. 2022. Does biochar affect soil wettability and flow pattern? Geoderma. 417:115826. https://doi.org/10.1016/j.geoderma.2022.115826
Major J. 2010. Guidelines on practical aspects of biochar application to field soil in various soil management systems *Rep*. International Biochar Initiative.
Mohamed MM, Raghunandan ME. 2025. Impact of biochar on the compression and hydraulic conductivity of sands for engineering application. Int J Environ Sci Technol. 22(11):10383–10400. https://doi.org/10.1007/s13762-024-06296-y
Ng CWW, Guo H, Ni J, Zhang Q, Chen Z. 2022. Effects of soil–plant-biochar interactions on water retention and slope stability under various rainfall patterns. Landslides. 19(6):1379–1390. https://doi.org/10.1007/s10346-022-01874-y
Sharma P, Ali S, Biswas JK. 2025. Application of biochar for soil erosion control and environmental management: implications for achieving sustainable development goals. Discov Soil. 2(1):36. https://doi.org/10.1007/s44378-025-00065-0
Sun W-J, Li M-Y, Zhang W-J, Tan Y-Z. 2020. Saturated permeability behaviour of biochar-amended clay. J Soils Sediments. 20(11):3875–3883. https://doi.org/10.1007/s11368-020-02720-1
Sun Z, Yan X, Han W, Ma G, Zhang Y. 2019. Simulating the filtration effects of cement-grout in fractured porous media with the 3D unified pipe-network method. Processes. 7(1):46. https://doi.org/10.3390/pr7010046

Trifunovic B, Gonzales HB, Ravi S, Sharratt BS, Mohanty SK. 2018. Dynamic effects of biochar concentration and particle size on hydraulic properties of sand. Land Degrad Dev. 29(4):884–893. https://doi.org/10.1002/ldr.2906
Verheijen F et al. 2010. Biochar application to soils – a critical scientific review of effects on soil properties, processes and functions. JRC Publications. https://doi.org/10.2788/472
Wan Y et al. 2022. Effect of biochar on permeability of compacted soil and its microscopic mechanism. Can Geotech J. 59(12):2184–2195. https://doi.org/10.1139/cgj-2021-0586
Wang J, Su A, Liu Q, Zou Z. 2026. Effect of suction stress on the strength of rupture zone and stability of landslide. Sci Rep. 16(1):4609. https://doi.org/10.1038/s41598-025-34658-0
Wang Z et al. 2023. Analysis of the pore structure characteristics of saline soil in the profile within the frozen depth. Cold Reg Sci Technol. 212:103882. https://doi.org/10.1016/j.coldregions.2023.103882
Xu B, Zhang H, Yin J, Xue Y. 2023. Infiltration grouting mechanism of bingham fluids in porous media with different particle size distributions. Appl Sci. 13(21):11986. https://doi.org/10.3390/app132111986
Yang C et al. 2025. Spherical penetration grouting model for bingham fluids considering gravity and time-varying slurry viscosity. Int J Geomech. 25(2):04024339. https://doi.org/10.1061/IJGNAI.GMENG-10757
Yin J et al. 2022. Evaluation of long-term carbon sequestration of biochar in soil with biogeochemical field model. Sci Total Environ. 822:153576. https://doi.org/10.1016/j.scitotenv.2022.153576
Zhang J, Chen Q, You C. 2016. Biochar effect on water evaporation and hydraulic conductivity in sandy soil. Pedosphere. 26(2):265–272. https://doi.org/10.1016/S1002-0160(15)60041-8
Zhelnin M, Kostina A, Plekhov O, Levin L. 2020. Numerical simulation of cement grouting of saturated soil during a mine shaft sinking using the artificial ground freezing. Procedia Struct Integrity. 28:693–701. https://doi.org/10.1016/j.prostr.2020.10.080
Zhong Z, Li J, Bie C. 2023. Theoretical approach to predicting the diffusion radius of fracture grouting in soil–rock mixtures. Appl Sci. 13(8):4730. https://doi.org/10.3390/app13084730
Zhou M, Fan F, Zheng Z, Ma C. 2021. Modeling of grouting penetration in porous medium with influence of grain distribution and grout–water interaction. Processes. 10(1):77. https://doi.org/10.3390/pr10010077